TRIBHUVAN UNIVERSITY

INSTITUTE OF ENGINEERING

PULCHOWK CAMPUS

THESIS NO. PUL080MSGtE007

FEM Based Performance Evaluation of BBMSE Walls Under Static and Vehicle Surcharge Load Conditions

by

Kailash Giri

A THESIS
SUBMITTED TO THE DEPARTMENT OF CIVIL ENGINEERING
IN PARTIAL FULFILLMENT OF THE REQUIREMENTS FOR THE
DEGREE OF MASTER OF SCIENCE IN
GEOTECHNICAL ENGINEERING

DEPARTMENT OF CIVIL ENGINEERING

LALITPUR, NEPAL

APRIL, 2026

COPYRIGHT

TRIBHUVAN UNIVERSITY
INSTITUTE OF ENGINEERING
PULCHOWK CAMPUS
DEPARTMENT OF CIVIL ENGINEERING

The thesis titled "FEM-Based Performance Evaluation of BBMSE Walls Under Static and Vehicle Surcharge Load Conditions" prepared and submitted by Kailash Giri in partial fulfilment of the requirements for the degree of Master of Science in Geotechnical Engineering has been examined by us and is accepted for the award of M. Sc. in Geotechnical Engineering by Tribhuvan University.

The undersigned certify that they have read, and recommended to the Institute of Engineering for acceptance, a thesis entitled "FEM-Based Performance Evaluation of BBMSE Walls Under Static and Vehicle Surcharge Load Conditions" submitted by Kailash Giri in partial fulfillment of the requirement for the degree of Master of Science in Geotechnical Engineering.

Supervisor:
Asst. Prof. Dr. Ram Chandra Tiwari
Department of Civil Engineering
IOE, Pulchowk Campus

External Examiner:
Er. Prabhat Kumar Jha
Superintendent Engineer
Department of Road, MoPIT

Program Co-Ordinator:
Asst. Prof. Dr. Bhim Kumar Dahal
M.Sc. in Geotechnical Engineering
IOE, Pulchowk Campus

Date: April 27, 2026

DECLARATION

I hereby declare that this study titled "**FEM-Based Performance Evaluation of BBMSE Walls Under Static and Vehicle Surcharge Load Conditions**" is based on my original research work. Related works on the topic by other researchers have been duly acknowledged. I owe all the liabilities relating to the accuracy and authenticity of the data and any other information included hereunder.

Kailash Giri
080/MSGtE/007
MSc. in Geotechnical Engineering
Date: April 27, 2026

ACKNOWLEDGEMENTS

I would like to give my sincere thanks to my supervisor, Dr. Ram Chandra Tiwari, for his invaluable guidance and constant support throughout this study. His insightful suggestions greatly enhanced the quality of my research. This study would not have been possible without his expertise and motivation.

I would also like to acknowledge Professor Indra Prasad Acharya, Assistant Professor Dr. Bhim Kumar Dahal, Assistant Professor Dr. Santosh Kumar Yadav and Assistant Professor Dr. Basanta Raj Adhikari and entire Geotechnical Engineering Department at Pulchowk Campus. Their constant encouragement has been central in broadening my horizons and improving my studies.

I would like to thank Er. Biraj Ojha, as well. With his generous help in Plaxis modelling without which the study would have not been done technically.

I also want to say that the Department of Civil Engineering, Pulchowk Campus, IOE, provided me with a good research environment.

Lastly, I would like to thank my family and friends who have been very inspirational and supportive in my studies. Furthermore, I would like to thank everyone who directly or indirectly helped me to create this work.

Kailash Giri

Roll No: 080/MSGtE/007

ABSTRACT

Those retaining walls that are stabilized using the reinforcing element are known as Mechanically Stabilized Earthen (MSE) Walls. When the two MSE walls are close to each other with their backfills common and their backs facing each other, there exists some interaction between the two backfilled soil mass. Such kind of system of two MSE wall is called Back-to-Back Mechanically Stabilized Earthen Walls (BBMSEWs) (Juneja et al., 2025). Numerical modeling has been used for understanding the complex nature of such structures, that enables parametric studies, performance prediction, and optimization of the design. The finite element methods (FEM), particularly implemented through Plaxis software, dominate the field. Parametric studies consistently demonstrate the critical influence of reinforcement stiffness, length, and spacing on wall performance, while facing type and soil-reinforcement interaction significantly affect displacement patterns. Despite substantial progress in understanding of the isolated MSE walls, significant research gaps persist in case of BBMSEWs, including sparse application of discrete element methods, insufficient validation studies, and inadequate characterization of interface mechanics. This study aims to analyze the how the back-to-back walls influence each other, with respect to their distance, height and other parameters, and analyze the response of the system when the vehicular loadings occur. Interaction analysis, based on Plaxis 2D were performed for different W/H ratios: from largely spaced to closely spaced MSE walls. The results are were assessed in terms of horizontal wall displacements, shear strain contours, lateral pressure exerted on the facing and behind the reinforcement zone, and the tension on the reinforcing elements.

Keywords: BBMSEW, Mechanically Stabilized Earth Walls; Numerical Modeling; Finite Element Analysis; Constitutive Models; Geosynthetic Reinforcement; Parametric Studies; Validation Methods.

TABLE OF CONTENTS

LIST OF FIGURES

LIST OF TABLES

LIST OF ACRONYMS

2D	: Two Dimensional
BBMSE	: Back-to-Back Mechanically Stabilized Earth
c'	: Effective Cohesion
W/H	: Spacing-to-Height Ratio
$\Delta\varepsilon_v$	: Incremental Volumetric Strain
$\Delta\gamma_s$	: Incremental Deviatoric Strain
Δu	: Incremental Displacement
E	: Elastic Modulus / Young's Modulus
EA	: Axial Stiffness
EI	: Flexural Rigidity
EPDM	: Ethylene Propylene Diene Monomer
FEM	: Finite Element Method
FHWA	: Federal Highway Administration
FLAC	: Fast Lagrangian Analysis of Continua
FOS	: Factor of Safety
GRS	: Geosynthetic Reinforced Soil
H	: Wall Height
HDPE	: High-Density Polyethylene
IRC	: Indian Roads Congress
K	: Earth Pressure Coefficient
K_0	: At-Rest Earth Pressure Coefficient
K_a	: Rankine Active Earth Pressure Coefficient
L	: Reinforcement Length
LRFD	: Load and Resistance Factor Design
MSE	: Mechanically Stabilized Earth

M_{sf} : Strength Reduction Factor (phi–c reduction method)

PET : Polyethylene Terephthalate (Polyester)

R_{inter} : Interface Strength Reduction Factor

S_h : Horizontal Reinforcement Spacing

S_v : Vertical Reinforcement Spacing

T_{max} : Maximum Reinforcement Tensile Force

UDL : Uniformly Distributed Load

W : Inter-wall Spacing

W/H : Wall Spacing-to-Height Ratio

γ : Unit Weight

ν : Poisson's Ratio

ϕ' : Effective Angle of Shearing Resistance / Friction Angle

ψ : Dilatancy Angle

1 INTRODUCTION

1.1 Background

Mechanically Stabilized Earth (MSE) walls have emerged as an economical and efficient alternative to conventional gravity retaining structures. Friction and interlocking between soil particles and reinforcement elements is the fundamental mechanism, that create a coherent gravity mass capable of resisting lateral earth pressures.

Since their introduction in the 1960s by Vidal (1966), MSE walls have gained widespread acceptance in transportation infrastructure. Their advantages include reduced construction time, tolerance to differential settlements, elimination of deep foundations, economy, aesthetics and adaptability to various site conditions and thus have replaced conventional retaining walls in many cases. The global adoption of MSE technology has been accompanied by continuous evolution in design methodologies, material specifications, and construction practices.

When these MSE walls are in proximity to each other in order to retain the backfill in between them, the interaction effects take place due to the intersection of the failure plane of the retained fill. This system of two walls is called Back-to-Back MSE walls (BBMSEWs). They are used in approaches of bridges, ramp ways of flyovers (as in the case of Gwarko flyover), rockfall protection systems, earth dams, levees, and noise barriers. However, the behavior of BBMSEWs hasn't been studied enough.

1.2 Statement of the Problem

Because of fore mentioned advantages MSE walls have become a widely adopted solution in geotechnical engineering. Among the various configurations, Back-to-Back MSE (BBMSE) walls are increasingly employed in highway embankments, bridge abutments, and elevated roadway structures where space constraints make it necessary to place two opposing MSE walls in proximity. They have also been used as barriers to resist lateral forces from natural disasters such as floods, tsunamis, rock falls, debris flows, and avalanches (FHWA, 2009a, 2009b; Taylor et al., 2023). Despite their growing application, the static behavior of BBMSE walls under realistic vehicle load configurations remains insufficiently understood, particularly with respect to the interaction effects governed by the spacing between the two opposing wall systems.

Current design guidelines such as AASHTO and FHWA has offered little specific guidance on BBMSE wall design, mainly due to the simple geometric arrangement and

assumed loadings. They fail to consider the intricate stress distribution, reinforcement tensioning, lateral earth pressure changes and deformation mode when two MSE walls are separated by a shared reinforced fill zone under static vehicle loads. The distance between the back-to-back walls is a crucial factor in determining the degree of interaction, overlap, and independence between the reinforced fill zones, but no well-developed numerical framework has been provided to comprehensively assess this distance under different vehicle load arrangements (Benmebarek et al., 2016).

The primary source of operational stress in highway and transportation applications are vehicle loads. The vehicle loads (e.g. wheel loads, load geometry and location) dictate the magnitude and distribution of vertical stresses, horizontal earth pressures and the strain in the wall reinforcement. The interaction of these vehicle-induced stress fields from two back-to-back walls that are close to each other can significantly differ from that of isolated walls. Hence, a numerical assessment of the interaction between different vehicle load configurations and inter-wall spacing is critical to determine the true static design space of BBMSE systems.

Thus, a numerical investigation using PLAXIS 2D finite element software offers a reliable means of evaluating the performance of wall system. This research aims to characterize the structural response, identify critical spacing thresholds, and provide performance-based insights by systematically varying the spacing between the two back-to-back walls under static vehicle load, that enables economic, safer and more efficient design of BBMSE wall systems.

1.3 Research Objectives

The main motive of this study is to evaluate numerically, the performance of BBMSE walls under surcharge vehicle load condition using FEM software. It emphasizes on the influence of inter-wall spacing on the structural response of the wall system. To achieve this primary objective, the following specific objectives are identified:

a. To develop and validate a FEM model of BBMSE walls in PLAXIS 2D
b. To evaluate the effect of different wall spacing on the performance of BBMSE walls
c. To examine the combined effect of inter-wall spacing and surcharge vehicle load on wall interaction
d. To suggest performance-based recommendations for the design of BBMSE walls

1.4 Scope of the Study

The boundaries within which the numerical investigation of BBMSE walls is conducted is defined by the scope of the study which is confined to the following parameters, conditions, and assumptions:

1.4.1 Reference wall and geometric configuration

The study is based on a real, instrumented MSE wall documented by Cristelo et al. (2016) in Geosynthetics International. A detailed numerical investigation of an MSE wall constructed in a section of the Portuguese Highway A4 was conducted, connecting the northern cities of Amarante and Vila Real. The length of the wall is approximately 335 m, height ranging between 7 m and 12 m (Kongkitkul et al., 2010). The geometric, material and field data reported by Cristelo et al. (2016) serve as the primary basis for model development and validation in this study.

The study is conducted in two distinct stages with respect to wall geometry:

Stage 1: Validation Model

- The geometry, dimensions, and material properties of the wall are adopted directly from Cristelo et al. (2016) to develop and validate the FEM model in PLAXIS 2D against the field monitoring data and numerical results reported in that study.
- After validation of the model confirming the reliability and accuracy of model, the study proceeds to the parametric investigation.

Stage 2: Parametric Study Model

- Following validation, the wall height is reduced to a 6 m, comprising four prefabricated reinforced concrete facing panels each of 1.5 m height, to simplify the parametric investigation.
- This simplified and representative configuration allows for evaluation of BBMSE wall behavior across a range of inter-wall spacing-to-height ratios (W/H).

1.4.2 Material properties and constitutive modeling

All material properties, the field measurements and experimental data adopted from Cristelo et al. (2016), are as follows:

Foundation Soil

- The jet grouting and cutter soil mixing (CSM) columns treatments were done to enhance bearing capacity of the foundation soil (Kongkitkul et al., 2010).
- Properties of the homogenized soil-column composite: elastic modulus E = 1.5 GPa, bulk density $\gamma = 20$ kN/m^3, cohesion $c' = 400$ kPa, dilatancy angle $\psi = 0°$, Poisson's ratio $\nu = 0.2$, and angle of shearing resistance $\phi' = 0°$ (Kongkitkul et al., 2010).

Reinforced Backfill

- The backfill is a frictional silty-sand with E = 60 MPa, $\psi = 10°$, $\nu = 0.3$, and $\phi' = 36°$, as characterized by Cristelo et al. (2016).
- The fines content (sieve #200) is 9% and the plasticity index is below 6%, making it suitable for use as backfill.
- The bulk unit weight after compaction is 18.0 kN/m^3, based on modified Proctor test results, yielding a maximum dry unit weight of 18.3 kN/m^3 at an optimum water content of 9.8%.

Retained Fill

- The retained fill properties are taken equal to those of the original untreated foundation soil: E = 15 MPa, $\gamma = 16.5$ kN/m^3, $c' = 10$ kPa, $\psi = 0°$, $\nu = 0.35$, and $\phi' = 25°$.

Constitutive Model

- Mohr-Coulomb elastoplastic constitutive model is used for modelling soil, as it provides a reasonable representation of soil behavior under the stress levels encountered in the reference wall.
- The constitutive models such as Hardening Soil or Soft Soil Creep are not considered in this study due to insufficiency of the parameters.

1.4.3 Reinforcement

- The wall is reinforced using polyester strip reinforcements encased in a knurled polyethylene sheath, each reinforcement strip having a cross-sectional area of 0.092 m × 0.0023 m and a design tensile strength of 30 kN.
- Reinforcement strips of 10.5 m length are installed at vertical intervals of 0.75 m and horizontal intervals of 0.5 m and are modeled as

equivalent elastoplastic geogrid elements, as per the reference document.

- For the parametric model, the length of the strips is adopted as 0.7H, as per the FHWA guidelines.(Berg et al., 2009)
- All other parameters are kept constant across all spacing configurations to isolate the effect of inter-wall spacing.

1.4.4 Facing panel

- The wall facing of width of 2.25 m, height of 1.5 m (first six panels) and 2.375 m (top panel), and thickness of 0.15 m consists of prefabricated reinforced concrete panels with the following dimensions (Cristelo et al., 2016).
- E of 30 GPa and poisons ratio, ν of 0.20 are facing panel material properties.
- To prevent the direct contact between panels and avoid point stress, ethylene propylene diene monomer (EPDM) joints of 20 mm thickness are provided. It is covered with a geotextile filter to prevent fine material loss, consistent with the reference wall construction (Kongkitkul et al., 2010).
- They are modeled as linear elastic plate elements in PLAXIS 2D.

1.4.5 Loading conditions

- To simulate the effect of highway vehicular traffic, equivalent static surcharge loads is applied at the wall crest based on the suggestion of AASTHO LRFD guidelines (AASTHO & Caltrans, 2017).
- Vehicle loads are not modeled as moving loads in the static analysis

1.4.6 Numerical modeling platform

- PLAXIS 2D FEM software is used for all the numerical analyses.
- The study does not employ 3D FEM, limit equilibrium methods as primary analysis tools, though findings from such approaches available in the literature are used for model validation and result comparison (Cristelo et al., 2016; El-Sherbiny et al., 2013; Han & Leshchinsky, 2010).

1.4.7 Performance indicators

To evaluate the performance of the BBMSE system, the following output parameters are used:

- Distribution of the horizontal earth pressure along the wall facing and behind reinforcement zone
- Reinforcement tensile forces at various levels
- Lateral Wall Displacement
- Distribution of plastic points
- Shear strain contours and critical failure lines

1.4.8 Model validation

- The field monitoring data and numerical results reported by Cristelo et al. (2016) is used for the validation of FEM model.
- Additional comparison is made with the numerical findings of previous literature where applicable. (El-Sherbiny et al., 2013; Won & Kim, 2007)

1.5 Limitations of the Study

The following aspects are outside the scope of this study:

- Seismic loading is not considered.
- 3D effects of vehicle configurations, such as out-of-plane load distribution and wheel-path geometry, are not modeled.
- Long-term creep behavior of polyester reinforcement strips and time-dependent soil deformation are not considered. Also, degradation or durability of the polyethylene sheath encasing the polyester reinforcement strips is not examined.
- Hydraulic effects such as pore water pressure buildup, consolidation, and drainage conditions, are not considered; fully drained conditions are assumed throughout the study.
- The design optimization of BBMSE wall components such as reinforcement length, facing panel dimensions, or foundation treatment is not done.
- The properties of composite jet grouting and CSM column treatment of the foundation is accounted using equivalent parameters reported by Cristelo et al. (2016); detailed modeling of individual columns is not done.

2 LITERATURE REVIEW

2.1 Introduction to MSE Walls

The concept of Reinforced Earth was pioneered by a French engineer and architect Vidal in the 1960s. He finds out that the tensile properties of earth can be significantly improved by the insertion of tensile elements within a granular fill mass. The tensile property enhances the shear strength and stability of the composite earth material. This discovery resulted the conceptual foundation for what is now broadly referred to as Mechanically Stabilized Earth (MSE) (Vidal, 1966).

The first full-scale application of Vidal's concept was done in 1965 at Provo, Utah, in the United States, and in the Rhône Valley in France (Mitchell & Villet, 1987). The successful performance of these early structures triggered widespread interest among geotechnical engineers suggesting the viability of the concept. The introduction of geosynthetic reinforcement materials in the late 1970s and 1980s transformed MSE wall technology. Researches in that period made significant contributions in understanding the mechanics of geosynthetic-reinforced soil systems. It led to the development of design frameworks that could accommodate a wide range of reinforcement types and soil conditions. (Binquet & Lee, 1975; Jewell et al., 1984) The FHWA published its first comprehensive design manual for MSE walls in 1996, with the most recent edition published in 2009. (Berg et al., 2009).

Decades after, innovations in reinforcement materials, facing systems, and construction techniques evolved MSE wall technology, further expanding the applications of these structures. Today, MSE walls are one of the most commonly constructed earth retaining structures worldwide. (Elias et al., 2001)

2.2 Components and Behavior of MSE Walls

The performance and structural integrity of a MSE wall are fundamentally dependent on the properties of its constituent components and their interaction under applied loading. An MSE wall system is composed of three major components, the reinforced fill, the tensile reinforcement elements, and the facing system. Each component contributes in a unique way to the overall behavior of the wall. The performance of the system as a whole is a function of the complex interactions developed between the components during and after construction. The rational design, construction and performance evaluation of MSE wall systems require a clear understanding of the individual behavior of each component, and of their collective interaction.

2.2.1 Reinforced fill

The biggest volumetric component of an MSE wall is the reinforced fill. It is the medium through which the applied loads are transferred to the reinforcement elements. The mechanical properties of the fill, such as its shear strength, stiffness, unit weight and drainage characteristics have a direct effect on the magnitude of the lateral earth pressures acting on the facing, the available pullout resistance along the reinforcement and the overall deformation behavior of the wall system. Therefore, selection and quality control of reinforced fill material is one of the most important aspects in MSE wall design and construction (Wu, 2019).

2.2.2 Reinforcement elements

Based on material composition and mechanical behavior, reinforcement are of two types: inextensible metallic reinforcements and extensible geosynthetic reinforcements. Metallic Reinforcements include galvanized steel strips, ribbed steel strips, bar mat reinforcements, and welded wire grids. They have high tensile modulus, negligible creep under sustained load, and high durability. But it should be properly protected against corrosion. Galvanized steel strips, which was used by Vidal (1966), remain widely used in highway MSE wall. The primary load transfer mechanism for smooth metallic strips is interface friction, which depends on surface characteristics of the strip and the properties of the surrounding fill. Mechanical interlocing can also be introduced such as in case of ribbed or textured metallic strips (Schlosser & Long, 1974).

Geosynthetic Reinforcements includes a wide range of polymer-based products, such as woven and nonwoven geotextiles, uniaxial and biaxial geogrids, and composite geocomposites. Geotextiles transfer load to the surrounding soil mainly through interface friction, while geogrids mobilize load transfer through both interface friction along their longitudinal members and passive bearing resistance of their transverse members against the confining soil (Jewell et al., 1984). In stiff and widely spaced transversed membered geogrid, passive bearing resistance component is significant and provides substantial total pullout resistance developed in coarse-grained fills. Koerner (2005) provided a comprehensive review of geosynthetic reinforcement types, load transfer mechanisms, and design approaches, noting that the selection of an appropriate reinforcement type depends on the specific application requirements, including design load, deformation tolerance, durability requirements, and economic constraints.

The VSL FASTEN polyester strip system used in the Portuguese Highway A4 wall documented by Cristelo et al. (2016). It combines the high tensile strength of polyester filament yarns with the corrosion resistance and surface friction of a knurled polyethylene sheath. These systems maintain balance of structural performance and durability for highway MSE wall applications.

2.2.3 Facing systems

The facing system of an MSE wall provides structural confinement of the reinforced fill at the exposed face, prevents local raveling and erosion, transfers residual lateral earth pressures to the reinforcement elements. It provides aesthetic appearance. The type of facing system selected can influence on the overall stiffness of the wall, the distribution of earth pressures and reinforcement loads, and the deformation behavior of the wall under applied loading.

Precast concrete panel facings are the most widely used facing system for highway MSE walls. They are of standardized dimensions typically cruciform, rectangular, or hexagonal in shape, erected in alternating courses as fill placement progresses. The reinforcement elements are connected to panels through embedded steel connectors, and bearing pad between adjacent panels accommodate differential settlements and other movements without cracking.

The stiffness of the facing system has a significant influence on the distribution of reinforcement loads and lateral earth pressures within the MSE wall. Rowe & Ho (1998) showed through FEM analyses that stiffer facing systems supports a greater proportion of the lateral earth pressure and thus reduce the tension on reinforcement. In a comprehensive experimental and numerical study, Bathurst et al. (2000) showed the influence of facing stiffness on the behavior of geosynthetic reinforced soil walls. They found that walls with rigid concrete panel facings showed significantly lower tension and horizontal deformations than walls with flexible wrapped facings under identical conditions implying that the use of a stiffer facing system can provide an additional FOS against reinforcement overstress, but at higher material cost.

Ling et al. (1997) used FEM modeling to investigate the interaction between the facing panel and the reinforcement connection under lateral earth pressure loading. They found that the connection detail particularly the eccentricity of the reinforcement attachment point relative to the panel centroid significantly influences the bending moment distribution within the panel and the tension in the connecting hardware.

These findings highlighted the importance of careful detailing of the facing-reinforcement connection in the structural design of MSE wall facing panels.

2.3 Back-to-Back MSE Walls

As the application of MSE walls has expanded, there arises the situations where two opposing MSE walls must be constructed closely to one another, sharing a common reinforced fill zone between them. Such system is known as a Back-to-Back MSE (BBMSE) wall. It occurs often in the construction of elevated highway embankments, ramps of interchange, bridge approach, and overpasses, where space constraints, or topographic conditions necessitate the use of two opposing retaining walls in proximity (Sravanam et al., 2019). All the fundamental components of BBMSEWs are same as single MSE walls. But their structural behavior is quite different, owing to the interaction that develops between the two opposing reinforced fill zones when the walls are placed in sufficiently close proximity (Berg et al., 2009).

The degree of interaction between the two opposing walls is primarily governed by the spacing between the two wall facings, typically expressed as a ratio of the clear distance between the facings (W) to the height of the wall (H), giving the dimensionless parameter W/H. When this ratio is large, the two walls behave essentially as independent structures. However, as the spacing decreases and the W/H ratio falls below a critical threshold, the reinforced fill zones of the two walls begin to interact, the failure wedges of the opposing walls overlap or interfere with one another. The assumptions underlying conventional single-wall design methods diverges (Djabri & Benmebarek, 2016). Understanding the nature of this interaction and its effect in stress distribution, reinforcement behavior, and stability of the wall system is the primary motivation for the present study.

A BBMSE wall system consists of two MSE walls constructed with their facing elements oriented in opposing directions, separated by a distance W measured between the two facing surfaces. The reinforcement elements of each wall extend horizontally into the shared fill zone between the two facings. The reinforcement layers of the two opposing may or may not overlap, depending on the reinforcement length and the inter-wall spacing. The total width of the BBMSE wall system encompassing both reinforced fill zones and any unreinforced fill between them is therefore a function of the reinforcement length on each side and the clear spacing between the facings.

Taylor et al. (2023) defined the four different layouts of geometric configurations of BBMSE walls in the FHWA design guidelines depending on the distance between the faces of two opposing walls, L_w, and the back distance (distance between the ends of the reinforcement), D, as shown in figure:

2.3.1 Case I:

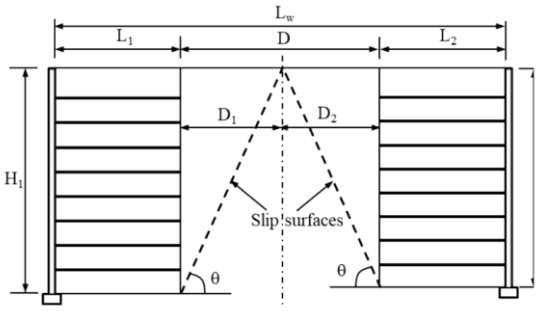

Figure 2.1: Configuration of case I adopted from Taylor et al. (2023)

When these distances are large enough, the two opposing walls perform independently and can be designed as one-sided MSE walls. Such walls are not considered BBMSE walls. They are considered to act as independent MSE walls in terms of external stability when the back distance, D, satisfies the following condition:

$$D = D_1 + D_2 \geq \frac{H_1 + H_2}{\tan(\theta)}$$

Where:

D_1 = top slip surface distances behind the reinforced zones from Wall 1 (taller wall)

D_2 = top slip surface distances behind the reinforced zones from Wall 2 (shorter wall)

H_1= height of Wall 1

H_2 = height of Wall 2

θ = angle of potential planar slip surfaces from the horizontal behind the reinforced zones at an active state

The angles of the potential planar slip surfaces in the retained soil may be determined using the Coulomb or Rankine earth pressure theory. When the Rankine theory is used, the angles are equal to, $\theta = 45° + \frac{\varphi_b}{2}$, where φ_b is the friction angle of the retained fill.

2.3.2 Case II:

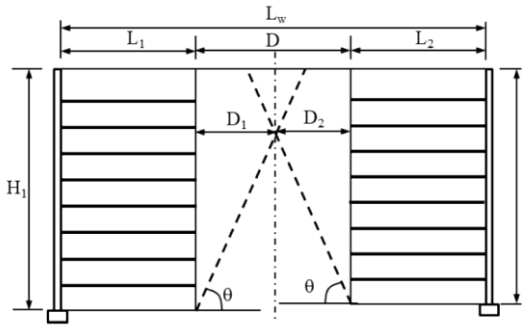

Figure 2.2: Configuration of case II adopted from Taylor et al. (2023)

When the potential slip surfaces behind the reinforced zones interact, as shown in Figure 98b, the back distance, D, is:

$$0 < D \leq \frac{H_1 + H_2}{\tan(\theta)}$$

2.3.3 Case III & IV:

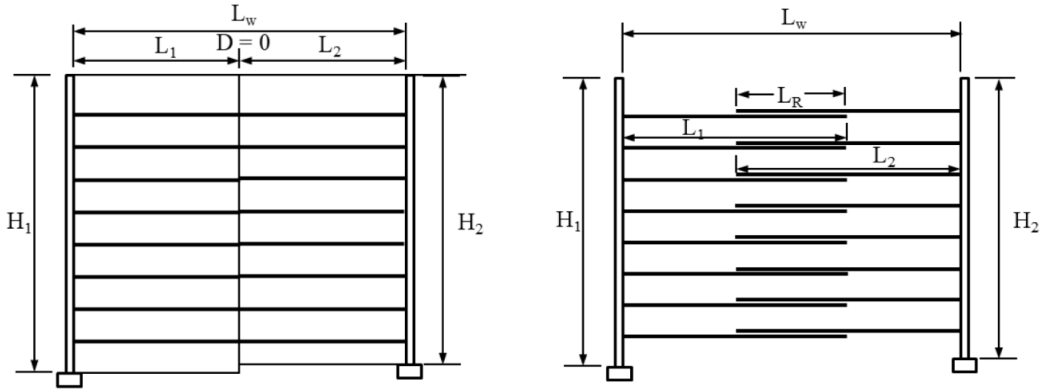

Figure 2.3: Configuration of case III and IV adopted from Taylor et al. (2023)

These are the cases where BBMSE reinforcement from the two walls meet in the middle as or overlap as shown in the above figures.

2.4 Design Guidelines for BBMSE Walls

In a BBMSE wall system with small inter-wall spacing the failure wedges of the two opposing walls may interfere with or overlap each other, preventing the full development of the active failure wedge in either wall. Han & Leshchinsky (2010) were among the first researchers to systematically investigate this interaction

phenomenon using limit equilibrium analysis. Their study showed that for W/H ranging from 2 to 3, the critical failure surfaces of the two opposing walls still interact with each other at the limit equilibrium state (FS = 1). The lateral earth pressure distribution within a BBMSE wall system differs significantly from that in a single isolated MSE wall, particularly when the inter-wall spacing is small. In a single MSE wall, the horizontal earth pressure at any depth is conventionally estimated as K_a times the vertical overburden stress, giving a triangular distribution with depth. But for BBMSEWs, the mutual confinement of the two opposing fill zones modifies pressure distribution (Brouthen et al., 2022).

El-Sherbiny et al. (2013) investigated the earth pressure distribution in BBMSE walls using FEM. Their study showed that when the spacing-to-height ratio D/H is less than 1, the earth pressure behind each wall decreases relative to the single-wall case. This means that assumption of full active earth pressure mobilization in conventional design methods may overestimate the reinforcement loads in closely spaced BBMSE configurations.

The most comprehensive design guideline of MSE wall systems was the FHWA Design and Construction of Mechanically Stabilized Earth Walls and Reinforced Soil Slopes manual, published by Berg et al. (2009). FHWA manual contains comprehensive guidelines of internal and external stability design of MSE walls under both static and seismic loading conditions. a variety of wall geometries, reinforcement types and facing systems is discussed. Special configurations such as back-to-back walls, tiered walls, sloping walls, and bridge abutment walls have the FHWA manual in place to offer additional guidance that alters the single-wall design routines to take into account the behavioral peculiarity of each set-up.

The FHWA design system of MSE walls is founded on a limit equilibrium design. the mass of the reinforced fill is considered to be a rigid body and the internal and external stability of the wall is considered against a proposed set of defined failure modes. The individual reinforcement layers design is founded on the premise that the horizontal earth pressure at a given depth in the reinforced fill is equal to the active Rankine earth pressure which is calculated using the active earth pressure coefficient K_o, based on the active earth pressure coefficient on the reinforced fill friction angle. This horizontal earth pressure multiplied by the tributary area of fill of that reinforcement layer is then considered to be the maximum tensile force in that reinforcement layer. the reinforcement is such that it can withstand the horizontal

earth pressure with sufficient factors of safety against tensile rupture and pullout failure.

The FHWA manual adopts the Simplified Method as the standard internal stability design procedure for MSE walls. It assumes lateral earth pressure coefficient is vary linearly with depth. This simplified pressure distribution is a pragmatic simplification of the more complex stress state that develops in reality, and its accuracy has been validated against a substantial body of instrumented field wall data for single isolated MSE walls. However, its applicability to BBMSE wall systems where the stress state is modified by the interaction between opposing fill zones has not been sufficiently studied. This represents a significant limitation of the current FHWA design framework for back-to-back configurations.

2.5 Numerical Modeling

The stress-deformation behavior of MSE wall systems is complex. It is characterized by nonlinear soil behavior, soil-reinforcement interaction, staged construction effects, and the influence of applied loading on internal stress distributions. It makes analytical solutions inadequate for the realistic prediction of wall performance. Numerical methods have therefore been popularly used as the primary tool for the rigorous analysis of MSE wall systems.

The FEM is the method adopted in the present study. In the FEM approach, the problem domain encompassing the reinforced fill, retained fill, foundation soil, reinforcement elements, and facing system is discretized into a mesh of finite elements. Each of them is assigned appropriate material properties and constitutive relationships. The governing equations of equilibrium, compatibility, and constitutive behavior are assembled into a global system of equations. Then those equations are solved numerically to obtain the displacement, strain, and stress fields throughout the problem domain under the applied loading and boundary conditions.

The application of the FEM to reinforced soil structures was pioneered by Clough & Duncan (1971). They used a 2D model to analyze the behavior of retaining walls and showed the importance of construction sequence and soil nonlinearity in governing wall behavior. Subsequent developments by Naylor (1982), and others established the FEM as a reliable tool for the analysis of reinforced soil structures that laid the foundation for the extensive body of numerical studies that has been done over the following decades.

There are significant benefits of the FEM in the analysis of MSE walls. It is able to support complex geometries, heterogeneous material behavior, and nonlinear constitutive behavior under one framework. It can directly model the stepwise construction sequence involving the incremental placement and compaction of fill layers and the insertion of reinforcement components that has been demonstrated to have a strong impact on the initial stress state and subsequent behavior of the wall. It is able to simulate the interaction between soil and reinforcement by using interface elements that record relative displacement and transfer of forces between the soil and the reinforcement. And it can give detailed data on the distribution of stresses, strains and displacements in the entire wall system, including reinforcement tensile forces, facing deformations, and earth pressure distributions, which are of interest in the primary performance evaluation of walls (Won & Langcuyan, 2020).

Constitutive Models for Soil Behavior

The constitutive model is needed to model the stress-strain behavior of the soil materials. It is crucial in determining the accuracy of a FEM model of an MSE wall system. Various constitutive models have been used in previous numerical analyses of MSE walls. It includes simple linear elastic models, and complex elasto-plastic models that model the nonlinear, stress-dependent, anisotropic behavior of actual soils.

The MC elastoplastic constitutive model is the most used soil model in FEM analyses of MSE walls, due to simplicity, physical interpretability, and reasonable accuracy for a broad range of problems. This model represents the soil as a linear elastic material below the yield surface. The yield surface is defined by the MC failure criterion in terms of the cohesion, c' and friction angle, ϕ' and as a perfectly plastic material at yield. The plastic flow is governed by a non-associative flow rule characterized by the dilatancy angle, ψ.

The MC model requires five input parameters: the elastic modulus E, Poisson's ratio ν, cohesion c', friction angle ϕ', and dilatancy angle ψ. These parameters are relatively straightforward to determine from standard laboratory and field tests and thus makes the the model particularly viable for practical engineering applications.

Hatami & Bathurst (2005) showed that the MC model provides reasonable predictions of reinforcement loads, facing deformations, and earth pressure distributions in GR soil walls in a condition that appropriate input parameters and initial stress conditions are used. El-Sherbiny et al. (2013) used the MC model in their

FEM analysis of BBMSE walls and achieved good agreement with the physical model test data of Won & Kim (2007). It confirmed the adequacy of this constitutive model. The MC model is adopted as the primary constitutive model for all soil materials in the present study.

In the PLAXIS, soil-reinforcement interaction is modeled through interface elements with a user-defined strength reduction factor R_{inter}. It reduces the interface friction angle and cohesion relative to the surrounding soil properties.

2.5.1 PLAXIS 2D as a numerical modeling tool

PLAXIS 2D is one of the most widely used and well-tested numerical platforms for the analysis of geotechnical engineering problems. It features a complete set of constitutive models, structural element types and analysis procedures. All these are bundled in a user-friendly interface that is suitable for both routine engineering practice and advanced research applications.

For 2D analyses, PLAXIS 2D uses a plane strain or axisymmetric finite element formulation. The plane strain assumption is the standard assumption used for the analysis of retaining walls and MSE walls because of the large length of the wall compared to its cross-sectional dimensions. In PLAXIS 2D, the basic soil elements are the six-noded and the fifteen-noded triangular elements. The fifteen-node element is based on a fourth-order interpolation of displacements and a third-order variation of stresses and strains in each element.

2.5.2 Meshing

The mesh generation in PLAXIS 2D is largely automated, with the software generating an unstructured triangular mesh based on user-defined geometry and a target global mesh coarseness level ranging from very coarse to very fine. Brinkgreve et al. (2012) recommended the use of a medium to fine global mesh for most MSE wall analyses. the local refinement is applied to the reinforcement layers and interface zones to capture the high stress gradients that develop in these regions. Hatami & Bathurst (2005) conducted a mesh sensitivity study for their FDM analyses of GRS walls and discovered that the predicted reinforcement loads and facing deformations converged with decreasing element size. It thus recommends a minimum of four to six elements per reinforcement spacing to achieve good results. These guidelines are chosen in this study for the design of mesh for both the validation model and the parametric study models.

2.5.3 Boundary condition

For MSE wall analyses in PLAXIS 2D, the standard boundary conditions consist of fixed vertical and horizontal displacements at the base of the model. It represents the rigid foundation boundary. The fixed horizontal displacements at the lateral model boundaries represents the plane of symmetry or the far-field boundary and free surface conditions at the top of the model where loads are applied. The lateral extent of the model domain must ensure that the boundaries do not influence the stress distribution and deformation behavior in the zone of interest.

2.5.4 Plate elements

Plate elements in PLAXIS 2D are one-dimensional structural elements that model the bending and axial behavior of slender structural members such as retaining walls, sheet piles, tunnel linings, and MSE wall facing panels. Plate elements are defined by their axial stiffness EA, bending stiffness EI, and unit weight w per unit length. They can sustain both tensile and compressive axial forces as well as bending moments and shear forces. The plate element formulation in PLAXIS 2D is suitable for the modeling of relatively thick structural members such as the precast concrete facing panels.

2.5.5 Geogrid elements

Geogrid elements in PLAXIS 2D are one-dimensional structural elements that model the axial tensile behavior of geosynthetic reinforcement layers. They can resist the tension but not the compressional forces. It is defined by its axial stiffness EA, which represents the tensile stiffness of the reinforcement layer per unit length of wall in the direction out of the plane of the model.

In the modeling of metallic strip reinforcements, the axial stiffness of the geogrid element is computed from the elastic modulus and cross-sectional area of the individual strips, divided by the horizontal spacing between strips to obtain the equivalent stiffness per unit width of wall.

2.5.6 Interface elements

Interface elements in PLAXIS 2D model the interaction between two materials at their common boundary that allows for relative displacement sliding and separation while transmitting normal and shear forces across the interface. Interface elements are essential for the accurate modeling of soil-reinforcement interaction, soil-facing interaction, and foundation-soil interaction in MSE wall analyses.

Interface elements in PLAXIS 2D are defined by a strength reduction factor R_{inter}, which reduces the interface friction angle and cohesion relative to the properties of the adjacent soil material as per the following relations:

$$tan(\delta) = R_{inter} \times tan(\phi'_{soil}) \quad (1)$$

$$c_{inter} = R_{inter} \times c'_{soil} \quad (2)$$

where δ represents interface friction angle and c_{inter} represents cohesion at the interface. The R_{inter} value attains the shear resistance reduced at the soil-reinforcement or soil-structure interface relative to the bulk shear strength of the soil. It represents the smoother surface of the reinforcement or structure compared to the surrounding fill.

2.6 Research Gaps

The behavior of individual MSE walls under surcharge loading has been broadly studied through field instrumentation programs including the seminal studies of Christopher et al. (1990); Cai & Bathurst (1995); Hatami & Bathurst (2005) and through numerical investigations using FEM and FDM. Current FHWA and AASHTO design provisions for BBMSE walls are based on simplified geometric criteria that have been shown to underestimate the true interaction distance.

The current landscape of BBMSE wall design reveals a significant gap between standardized guidelines and complex field realities. Existing literature on these systems often relies on theoretical derivations or small-scale laboratory experiments which fail to account for the subtle soil-structure interaction. Furthermore, there is a distinct lack of research that rigorously validates numerical models against instrumented field data before conducting parametric investigations.

This research addresses these deficiencies by developing a FEM model specifically calibrated using real-world instrumented field data. By utilizing actual field performance as a benchmark, the study provides a unique and reliable foundation for evaluating how varying inter-wall distances influence lateral earth pressure, reinforcement tension, and overall wall stability. Finally, this work tends to reduce the gap between academic theory and practical engineering by proposing performance-based design recommendations that account for overlapping reinforcement zones and the effects of static and vehicle surcharge loads.

3 METHODOLOGY

The overall research framework of the present study is structured on a static analysis. It serves a distinct purpose in the investigation of BBMSE wall behavior under operational highway loading conditions.

The static analysis aims to characterize the influence of inter-wall spacing on the structural behavior of BBMSE walls under single axle vehicle surcharge loading. This phase involves the systematic variation of the W/H ratio across five configurations, W/H = 1.2, 1.4, 1.7, 2.0, and 3.0 representing a range from closely interacting to effectively independent wall behavior. The performance of each BBMSE wall configuration is evaluated in terms of key structural response indicators. It includes lateral earth pressure distribution, reinforcement tensile forces, horizontal wall facing deformation, vertical stress distribution within the reinforced fill, etc.

All numerical analyses in the present study are performed using PLAXIS 2D finite element software. PLAXIS 2D is selected as the primary analytical tool for the following reasons. First, it provides a comprehensive and well-validated platform for the finite element analysis of geotechnical structures. It supports a wide range of constitutive models, structural element types, and analysis procedures specifically designed for soil-structure interaction problems. Second, its application to MSE and BBMSE wall analysis has been extensively validated in the literature. Also modeling approaches provides direct basis for the model developed in this study (Cristelo et al., 2016; El-Sherbiny et al., 2013).

The plane strain formulation of PLAXIS 2D is adopted. It assumes that the wall is of infinite length in the out-of-plane direction and that all deformations and stresses are uniform along the wall length. This assumption is considered appropriate for cross-sections remote from the wall ends. In such case the plane strain condition provides a reasonable approximation of the actual three-dimensional stress state. The single axle vehicle load is accordingly represented as an equivalent static strip load of uniform intensity in the plane strain analysis. The load magnitude and footprint width selected is to be representative of the standard single axle load specified in applicable highway design standards.

3.1 Stage 1: Model Development

3.1.1 Reference wall

The finite element model developed in the present study is based on the geometry, material properties, and construction sequence of the MSE wall in the Portuguese Highway A4 that connecting the northern cities of Amarante and Vila Real. The wall was constructed in 2010 by Infratúnel to provide lateral support to a section of highway traversing the hilly terrain of northern Portugal. It has a total length of approximately 335 m, with a height ranging between 7 and 12 m along its length. The instrumented section of this wall with a height of 11.4 m and 14 levels of reinforcement is adopted as the reference geometry for the validation model in the present study (Cristelo et al., 2016; Kongkitkul et al., 2010).

It is important to note that the Cristelo et al. (2016) wall is a single-faced MSE wall rather than a back-to-back configuration. In the absence of published experimental data from a representative instrumented BBMSE wall which is currently unavailable in the open literature, the Cristelo et al. (2016) single-wall field data is used as the validation reference for the present study. The validation exercise confirms the accuracy of the modeling approach, material parameters, and interface properties adopted in PLAXIS 2D before these are extended to the BBMSE configuration in the parametric study.

3.1.2 Model geometry

The reference wall geometry adopted for the validation model is constructed in PLAXIS 2D with the following components, directly consistent with the specifications reported by Cristelo et al. (2016):

- Wall height**:** 11.4 m, with 14 levels of reinforcement at 0.75 m vertical intervals.
- Reinforced fill zone**:** Represented by a soil mesh of height 11.4 m and reinforcement length of 10.5 m in each level.
- Model length of backfill soil**:** Extended to a distance of 30 m from the wall facing.
- Facing panels**:** Precast RC panels of 2.25 m width, 1.5 m height for the bottom six panels and 2.375 m for the top panel, and 0.15 m thickness, with EPDM joints of 20 mm thickness between consecutive panels.

- Levelling pad**:** Non-reinforced concrete of 0.15 m height and 0.30 m width at the base of the wall facing, serving as a foundation as well as guide for panel installation.
- Front fill**:** 0.5 m height of the same material as the reinforced backfill.
- Reinforcement strips**:** VSL FASTEN high-tenacity polyester strip reinforcement of 10.5 m length. It is installed at vertical spacing of 750 mm and horizontal intervals of 500 mm. Each reinforcement strip had a cross-sectional area of 92 mm × 2.3 mm and a design strength of 30 kN (Cristelo et al., 2016).
- Foundation soil**:** Jet grouted and CSM column treated, modeled using the homogenized composite properties determined from in-situ load testing.

The model back boundary extends to a distance of 30 m from the wall facing. It ensures that the lateral boundaries do not influence the stress distribution and deformation behavior in the zone of interest.

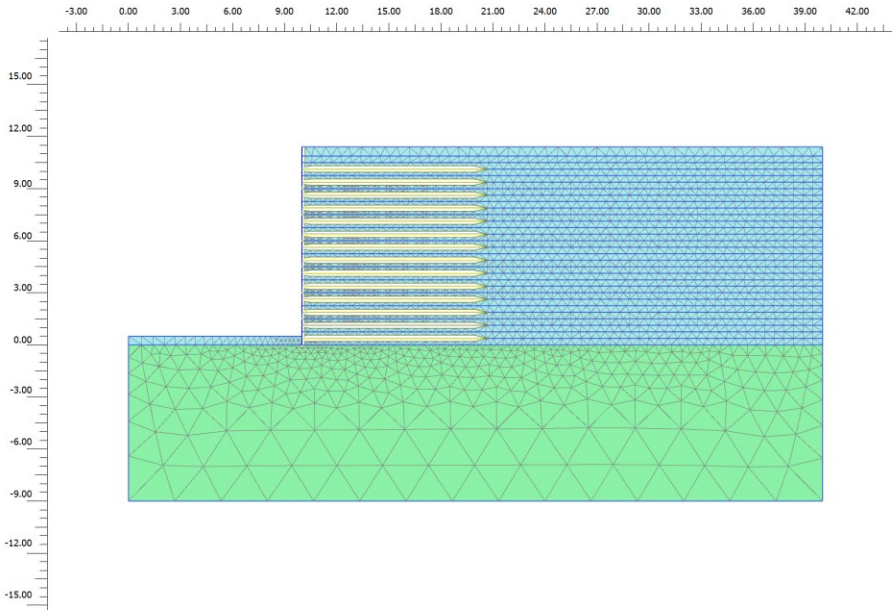

Figure 3.1: Connectivity plot of the MSE wall on Plaxis 2D

3.1.3 Finite element mesh

The soil mass having the reinforced and retained fill, and foundation soil is discretized into six-noded triangular elements in the PLAXIS 2D model. It is consistent with the element type adopted by Cristelo et al. (2016) in the reference model. A medium global mesh coarseness is adopted for the general soil domain which is selected on the based on the literature of Brinkgreve et al. (2012), who demonstrated that a

medium mesh provides enough numerical accuracy at the same time provides computational efficiency for analyses. It thus minimizes both calculation time and discretization error without the need for excessively fine global meshing.
Local mesh refinement is applied to the reinforcement elements, the interfaces at soil-reinforcement, and the facing panel elements to capture the high stress gradients that develop in these critical regions (Cristelo et al., 2016).

3.1.4 Material properties and constitutive models

All material properties are taken directly from the field instrumentation data which is summarized below. The MC elastoplastic constitutive model is adopted for all soil materials: the reinforced backfill, the retained fill, and the jet grouted foundation soil.

Table 3.1: Soil material properties adopted after Cristelo et al. (2016)

Material	**E (MPa)**	**ν**	**c′ (kPa)**	**ϕ′°**	**ψ°**	**γ (kN/m³)**
Foundation soil (jet grouted/CSM)	1500	0.2	400	0	0	20
Reinforced backfill (silty-sand)	60	0.3	0	36	10	18
Retained fill	15	0.35	10	25	0	16.5
Pavement (20cm thick linear elastic model)	3500	0.35				23

The linear elastic model is adopted for all structural elements, with properties as summarized as below.

Table 3.2: Structural element properties after Cristelo et al. (2016)

Element	**PLAXIS Element Type**	**Properties**
Facing panels	Three-node beam (plate)	E = 30 GPa, ν = 0.20
EPDM bearing pads	Three-node beam (plate)	EA = 533.3 kN/m, EI = 0.321 kNm²/m, ν = 0.495
Reinforcement strips	Geogrid (flexible element)	E = 5500 MPa, EA = 4 × 1163.8 = 4655 kN/m, design tensile strength = 4 × 30 = 120 kN/m
Levelling pad	Six-node triangular element	E = 25 GPa, ν = 0.20, γ = 24 kN/m³

The EPDM bearing pads between consecutive concrete panels are modeled as plate elements. The connections between the bearing pads and the concrete panels are modeled zero rotational stiffness hinges, allowing free rotation between adjacent panels (Cristelo et al., 2016; Kongkitkul et al., 2010). The reinforcement strips are modeled as geogrid elements with an elastic modulus of E = 5500 MPa. The value corresponds to the secant modulus at 1% strain specified in the VSL FASTEN technical documentation. This value is selected because the strain levels measured by all four strain gauges installed on the reinforcement strips were below 1%. It makes the most appropriate stiffness representation for the working strain range of the wall. None of the creep effects are included in the definition of the reinforcement axial stiffness. Third, each reinforcement strip consists of two layers of polyester bundles, and four strips are installed per meter of wall width at each reinforcement level. It gives a total axial stiffness of 4 × 1163.8 = 4655 kN/m per meter of wall (Cristelo et al., 2016).

3.1.5 Soil compaction

Soil compaction effects are not explicitly modeled in the present study. compaction during fill placement generates residual horizontal stresses that can influence the initial stress state of the reinforced fill. but these compaction-induced stresses are progressively diminished by the increasing overburden stress as subsequent fill layers are placed above. Seed et al. (1986) demonstrated that the effect of compaction on the stress state of the fill is effectively overridden by the overburden stress of the overlying fill layers toward the end of staged construction. It makes acceptable to neglect compaction effects in the initial stress state of the model without significant loss of accuracy in the predicted reinforcement tensions and facing deformations (Benmebarek et al., 2016).

3.1.6 Interface elements

Zero thickness three paired interface elements are used to model the soil-reinforcement and soil-panel interactions in PLAXIS 2D (Kongkitkul et al., 2010). The interface elements adopt an elastoplastic behavior governed by the MC failure criterion, with the interface friction angle and cohesion reduced relative to the adjacent soil properties through the interface strength reduction factor R_{inter}, as per the following relationships:

$$tan(\phi_{inter}) = R_{inter} \times tan(\phi_{soil})$$

$$c_{inter} = R_{inter} \times c_{soil}$$

$$\psi_{inter} = 0 \quad if\ R_{inter} < 1;\ \psi_{soil}\ if\ R_{inter} = 1 \tag{3}$$

where ϕ_{inter} and c_{inter} are the interface friction angle and cohesion, ϕ_{soil} and c_{soil} are the corresponding soil properties, and ψ_{inter} and ψ_{soil} are the dilatancy angles of the interface and soil, respectively (Cristelo et al., 2016).

The R_{inter} values are assigned as follows:

- Soil-reinforcement interface**:** R_{inter} = 1.0, that represents perfect bonding between the soil and reinforcement (Cristelo et al., 2016).
- Soil-panel interface**:** R_{inter} = 0.3, consistent with the value adopted by Damians et al. (2013) for the concrete panel facing of the reference wall.

3.1.7 Boundary conditions

Classic boundary conditions are applied to the finite element model:

- Bottom boundary**:** Fixed horizontal and vertical displacements that represents the rigid foundation boundary provided by the jet grouted foundation soil.
- Lateral boundaries**:** Fixed horizontal displacements, representing the far-field boundary condition at the sides of the model domain.
- Top boundary**:** Free surface at which the vehicle surcharge loads are applied in the loading stages

3.1.8 Staged construction sequence

The construction of the reference wall is modeled using the Staged Construction calculation mode in PLAXIS 2D, replicating the actual construction sequence (Cristelo et al., 2016). The staged construction model comprises 29 stages, organized as follows:

- In stage 1 the foundation layer and the levelling pad is activated.
- In stages 2, 6, 10, 14, 18, 22 and 26, 0.375 m thick layer of backfill is activated along with the plate element of wall and respective soil-wall interface. The front soil layer is also activated in Stage 2. In all stages except Stage 2, the corresponding bearing pads are also activated.
- In stages 3, 7, 11, 15, 19, 23 and 27, a reinforcement element is activated, also the activation of a 0.375 m thick backfill layer above the reinforcement is done,

activation of the corresponding soil-wall interface, and both soil-reinforcement, top and bottom interfaces is activated.

- In stages 4, 8, 12, 16, 20, 24 and 28, a 0.375 m thick layer of backfill soil and its corresponding soil-wall interface.
- In stages 5, 9, 13, 17, 21, 25 and 29, Activation of one layer of reinforcing elements is done, activation of a 0.375 m thick backfill layer above the reinforcement, activation of the corresponding soil-wall interface, and both soil-reinforcement interfaces is done (Cristelo et al., 2016).

This 29-stage construction sequence represents the sequential placement of fill layers and the installation of reinforcement and facing components in the actual wall construction process. The data obtained from the fitted instruments long after the completion of the wall is not considered in the validation. It is because creep effects of the polyester reinforcement are not included in the numerical model (Cristelo et al., 2016).

The stress state prior to wall construction is established using the K_0 procedure in PLAXIS 2D, with the coefficient of earth pressure at rest computed from Jaky's formula: $K_0 = 1 - \sin(\phi')$.

3.2 Stage 2: Validation of the Model

The validation of the finite element model is done by comparing the numerical predictions of the PLAXIS 2D model with the field monitoring data reported by Cristelo et al. (2016) for the Portuguese Highway A4 MSE wall. The validation is performed under static construction loading conditions that is, under the self-weight of the fill layers placed during staged construction using the reference wall geometry. The comparison is made for the following three output quantities, selected to provide a detailed assessment of the model's predictive accuracy:

- Horizontal wall facing displacement profile**:** horizontal displacement distribution along the height of the wall facing. It is measured by inclinometers installed in the reference wall during construction and predicted by the plate element displacements in the model at corresponding construction stages.
- T_{max} distribution**:** the variation of maximum reinforcement tensile force with depth within the wall. It is measured by resistance strain gauges bonded to selected reinforcement strips in the reference wall and predicted by the peak

geogrid element axial forces in the PLAXIS 2D model at corresponding reinforcement levels.

- Distance of T_{max} from the wall facing**:** the position along each reinforcement layer at which the maximum tensile force is mobilized, extracted from the distribution of axial forces along the geogrid elements and compared with the measured strain gauge data from the reference wall.

These three validation quantities are chosen because they provide the most significant elements of MSE wall behavior the deformation of the facing. This provides a sufficient test of the model's ability to represent the behavior of the reference wall.

3.3 Stage 3: Model Adaptation for Parametric Study

Following successful validation of the reference wall model against the Cristelo et al. (2016) field data, the model geometry and construction sequence are adapted for the parametric study. The adaptation involves two principal modifications: the reduction of the wall height to a standardized 6 m configuration for the BBMSE parametric study, and the extension of the single-wall model to a back-to-back configuration. It is done by mirroring the adapted wall on the opposing side of the shared fill zone. This standardized wall height is selected to provide a computationally simple and geometrically representative configuration for the parametric investigation of BBMSE wall behavior across the five W/H ratios considered. The panel dimensions and reinforcement properties of the reference wall is same.

The key adaptations made to transition from the reference wall to the 6 m parametric study wall are as follows:

- Wall height**:** Reduced to 6 m, with four facing panels each of 1.5 m height
- Reinforcement layer numbers**:** Eight layers at 0.75 m vertical intervals within the 6 m wall height, same as spacing in the reference wall
- Reinforcement length**:** Maintained at a value proportional to the wall height. It is consistent with the L_R/H of 0.7 of the reference walls i.e. 4.2 m (Elias et al., 2001; FHWA, 2009a, 2009b; Taylor et al., 2023).

All material properties, constitutive model selections, interface parameters, and boundary conditions established during the validation stage are retained without modification.

3.3.1 BBMSE configuration

The adapted single-wall model is extended to a back-to-back configuration by constructing a mirror image of the 6 m wall on the opposing side of the shared fill zone. the two wall facings are oriented in opposing directions and is separated by the inter-wall spacing, W. The inter-wall spacing is varied systematically across the five W/H ratio configurations considered in the parametric study, W/H = 1.2, 1.4, 1.7, 2.0, and 3.0. It gives inter-wall spacings of W = 7.2, 8.4, 10.2, 12.0, and 18.0 m respectively for the 6 m wall height.

3.3.2 Construction sequence of parametric study model

The parametric study model employs a 19-stage construction and loading sequence. It is significantly simplified compared to the 29-stage validation model while retaining the essential features of the staged construction approach. Following the completion of the wall construction stages, a pavement layer of 20 cm thickness is activated at the top of the fill between the two wall facings. It represents the road pavement surface constructed above the BBMSE wall system. The pavement layer is modeled using the linear elastic constitutive model with the following properties:

- Elastic modulus: 3500 MPa
- Poisson's ratio: $\nu = 0.35$
- Unit weight: $\gamma = 23$ kN/m^3(Brouthen et al., 2022)

The vehicle surcharge loading is applied in Stage 18 as a uniform distributed surcharge of 12 kN/m^2 at the pavement surface. it represents the equivalent static live load of highway vehicular traffic on the BBMSE wall system (Brouthen et al., 2022). The final stage of the analysis sequence involves analyzing failure mechanisms using strength reduction method in PLAXIS 2D.

Table 3.3: Summary of the construction and loading sequence of the model

Stage	**Activity**	**Elements Activated**
1	Foundation layer and levelling pad	Foundation soil, levelling pad
2–16	Sequential construction of 6 m BBMSE wall	Fill layers, reinforcement geogrid elements, facing panel plate elements, EPDM bearing pad plate elements, interface

		elements activated progressively from base to top for both opposing walls
17	Pavement layer construction	Pavement layer linear elastic, ν = 0.35, γ = 23 kN/m^3, thickness = 0.20 m
18	Vehicle live load application	Uniform surcharge of 12 kN/m^2 at pavement surface
19	Factor of safety calculation	Phi-c reduction method strength reduction applied to all soil materials

Stage 4: Parametric Analysis

The static parametric analysis investigates five BBMSE wall configurations defined by the W/H ratios. It is selected to cover the range from strongly interacting to approaching-independent wall behavior to encompass the interaction thresholds identified in the existing literature.

Table 3.4: MSE wall configurations investigated in the static parametric study

Configuration	**W/H Ratio**	**Inter-wall Spacing W (m)**
C1	1.2	7.2
C2	1.4	8.4
C3	1.7	10.2
C4	2.0	12.0
C5	3.0	18.0

Performance Indicators

The performance of each BBMSE wall configuration under each vehicle load scenario is evaluated in terms of the following key structural response indicators:

- Horizontal Earth Pressure Distribution**:** the distribution of horizontal earth pressure along the height of the facing, compared between different W/H ratio configurations, load positions, and the single-wall reference case.

- Reinforcement peak Tensile Forces (T_{max}): the maximum tensile force in each of the eight reinforcement layers, extracted from the geogrid element axial forces. It is compared between configurations and load positions to see the influence of inter-wall spacing on the reinforcement load distribution.
- Horizontal Wall Facing Deformation**:** the horizontal displacement profile of the wall facing panel, extracted from the plate element displacements. It compared between configurations to assess the serviceability implications of inter-wall spacing.
- Critical Failure Surface Patterns, Plastic Points Distribution and Incremental Displacement Distributions.

4 RESULTS AND DISCUSSION

4.1 Introduction

The chapter illustrates the findings of the numerical study of the behavior of BBMSE walls. The chapter is organized according to the five-stage research methodology in Chapter 3. It flows in a sequence starting with the model validation results, leading to the findings on the parametric analysis results. The results are reported throughout the chapter in the baseline condition of the self-weight and in the vehicle surcharge loading condition. All the results are given in the wall facing of the left-hand wall of the BBMSE setup.

4.2 Model Validation

The validation of the PLAXIS 2D finite element model is conducted by comparing numerical predictions with the field monitoring data reported by Cristelo et al. (2016). The validation is performed under static construction loading conditions using the 29-stage construction sequence described in Chapter 3. It focuses on three output quantities: the horizontal wall facing displacement profile, the maximum reinforcement tensile force (T_{max}) distribution with depth, and the distance of T_{max} from the wall facing at each reinforcement level.

4.2.1 Horizontal wall displacement profile

Both the predicted and measured displacement profiles exhibit the characteristic bulging shape as shown in Figure 4.1. The horizontal displacement increases progressively from near-zero at the base of the wall constrained by the levelling pad resting on the stiff jet grouted and CSM treated foundation to a maximum value in the upper portion of the wall. It reduces slightly toward the wall crest. The near-zero displacement at the base of both profiles confirms that the foundation boundary condition is correctly represented in the numerical model. The convergence of the two profiles toward the wall crest indicates consistent behavior in the uppermost reinforcement layers. The overall shape of the predicted displacement profile is in good qualitative agreement with the measured profile throughout the full 11.4 m wall height. It confirms that the 29-stage construction sequence, the Mohr-Coulomb constitutive model, and the material parameters adopted from Cristelo et al. (2016) collectively provide a physically representative simulation of the construction-induced lateral deformation behavior of the reference MSE wall.

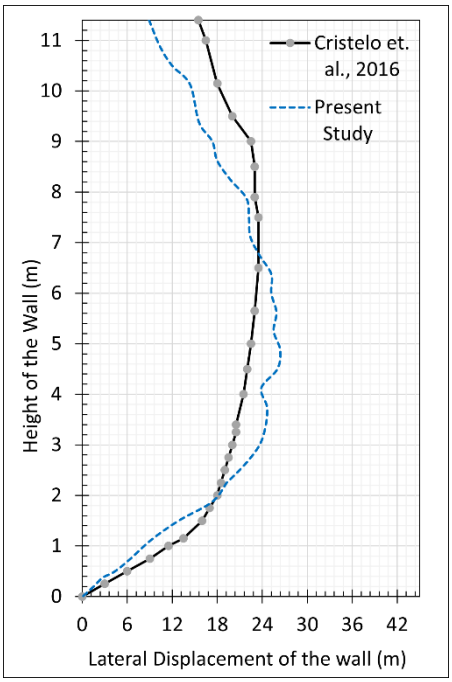

Figure 4.1: Lateral wall displacement of present study v/s *Cristelo et al. (2016)*

In quantitative terms, the measured maximum horizontal displacement reported by Cristelo et al. (2016) is approximately 24 mm, occurring at approximately H = 6.5 m up from the base of the wall. The numerically predicted maximum lateral displacement is approximately 26 mm, occurring at a similar elevation of approximately H = 5.0 m. The difference between the predicted and measured maximum displacements is therefore only 2 mm. It represents a percentage difference of approximately 8.3%. Throughout the height of the wall, the predicted and measured displacement profiles remain very close, with a margin of approximately 2 to 5 mm.

The maximum difference between the predicted and measured displacement values at any individual elevation across the full 11.4 m wall height is approximately 5 mm. It occurs in the topmost and mid-height region near H = 4.5 m. This maximum pointwise difference, while slightly exceeding 2 mm, remains well within the practical accuracy limits of field inclinometer measurements. It does not represent a meaningful discrepancy from a practical engineering perspective.

4.2.2 T_{max} distribution

Both the predicted and measured T_{max} profiles share the same general distribution pattern with depth as shown in Figure 4.2. It shows the highest tensile forces in the third lowermost reinforcement layer and decreasing progressively toward the upper

reinforcement levels. This lower-wall concentration of peak reinforcement tensions is in agreement with the classical active earth pressure behavior of MSE walls. Here the lateral earth pressure and reinforcement tension increases with depth due to the increasing overburden stress. This pattern is expected for the wall configuration modeled in the present study. The flexible facing system is above 1.5 m due to the zero rotational stiffness hinges modeled between adjacent panels that allows free rotation between panels and prevents the facing from attracting and redistributing lateral earth pressure toward the upper connection points.

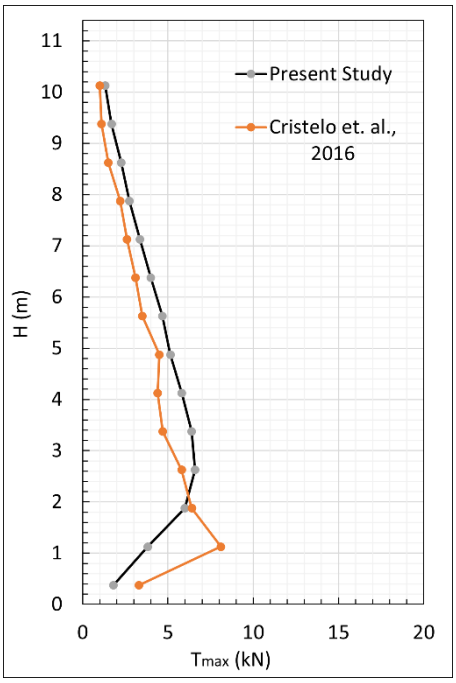

Figure 4.2: Comparison of the T_{max} with Cristelo et al. (2016)

The observed distribution of T_{max} along the wall height deviates from a linear hydrostatic increase at the base. It is due to a combination of external restraint and structural load redistribution. Firstly, the lateral support provided by the soil on the outer side of the wall acts as a passive resistance. It effectively counteracts a portion of the active earth pressure and reduces the tensile demand on the bottommost reinforcement layers. Secondly, the bottom facing panel's fixity at the leveling pad that extend up to 1.5 m, introduces a zone of high structural rigidity. It attracts lateral loads through cantilever action. This rigidity allows the panel itself to resist a significant portion of the soil pressure. It shields the lower geogrids and causing the maximum tensile forces to be transferred toward the leveling pad rather than being fully absorbed by the reinforcement.

Quantitively, the maximum T_{max} reported by Cristelo et al. (2016) is approximately 8 kN occurring at the second lowermost reinforcement layer. The maximum T_{max} predicted by the present numerical model is approximately 7 kN which occurs at the third reinforcement level from the base. Therefore, the absolute difference between the predicted and measured maximum T_{max} values is approximately 1 kN. It represents a percentage difference of approximately 12.5%.

While the magnitude of the maximum T_{max} is in good agreement, a notable difference is observed in the precise location of the peak tension within the lower portion of the wall. In the Cristelo et al. (2016) measurements, the maximum T_{max} occurs at the second lowermost reinforcement level. But in the present numerical model, the maximum T_{max} occurs at the third reinforcement level from the base, with slightly lower tensions at the two lowermost levels. These sources of localized discrepancy at the lowermost reinforcement levels are considered minor in the context of the overall validation. It does not affect the reliability of the model for the parametric investigation. The distribution of T_{max} across the full wall height rather than the precise location of the absolute maximum within the lower two or three reinforcement levels is the primary quantity of interest.

Throughout the remainder of the wall height from H = 2.0 m upward the documented and measured T_{max} profiles are in good agreement. Both profiles show a consistent and progressive decrease in reinforcement tension with increasing elevation. The predicted T_{max} values are slightly higher than the measured values by a margin of approximately 1 kN. In the uppermost reinforcement levels both the predicted and measured T_{max} values converge.

4.2.3 Distance of T_{max} from the wall facing

The observation from Figure 4.3 is the good agreement between the numerically predicted distances and the Cristelo et al. (2016) field measurements throughout the full 11.4 m wall height. Both the predicted and measured distance profiles are nearly coincident across all reinforcement levels, with both curves remaining consistently within 0 to 2 m from the wall facing. The two profiles follow each other closely at every elevation. It exhibits the same minor undulations and local variations in distance with depth. It confirms that the numerical model correctly locates the critical stress point the point of T_{max} within each reinforcement layer with high accuracy.

The consistently small distance of T_{max} from the wall facing remaining within 0 to 2 m across the full wall height for both the Cristelo et al. (2016) and measured profiles shows the influence of the flexible jointed facing system on the internal stress distribution. The EPDM bearing pads and zero rotational stiffness hinges between consecutive panels modeled, following the approach of I. Zevgolis & Bourdeau (2007), allow free rotation between adjacent panels. It prevents the development of a continuous rigid facing structure. This flexibility of the facing system means that the earth pressure acting on the facing is transferred directly to the reinforcement connection at each panel level rather than being redistributed over multiple panel heights through bending. It results in the concentration of the peak reinforcement tension at a point close to the facing connection. Therefore, the small and approximately constant distance of T_{max} from the wall facing observed across all reinforcement levels is a direct consequence of the flexible facing behavior. It is correctly reproduced by the numerical model through the explicit representation of the bearing pad plate elements and hinged connections.

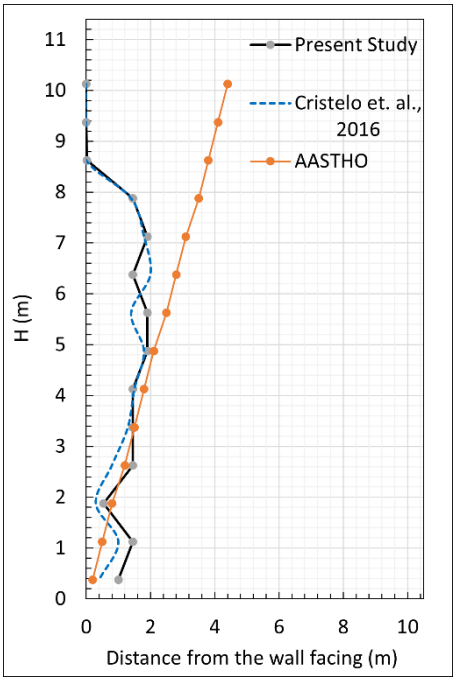

Figure 4.3: Comparison of the distance of T_{max} from the wall facing

Validation Summary

The successful validation of the PLAXIS 2D model against the Cristelo et al. (2016) field data across all three output quantities confirms the accuracy and reliability of the modeling approach adopted. The horizontal facing displacement profile is

reproduced with a maximum difference of only 2 mm equivalent to 8.3%. The T_{max} distribution is reproduced with a maximum difference of 1 kN equivalent to 12.5%. The distance of T_{max} from the wall facing is reproduced with excellent accuracy. The predicted and measured profiles are nearly coincident throughout the full wall height.

The validated material parameters, interface properties, reinforcement stiffness values, facing panel properties, and staged construction sequence are adopted without modification in all subsequent parametric study analyses. It ensures that the changes in wall behavior observed across the five W/H ratio configurations in the parametric study are attributable only to the variation in inter-wall spacing not to any change in the fundamental modeling assumptions.

4.3 Parametric Study

4.3.1 Horizontal wall displacement

The observation from the Figure 4.4 is that the lateral wall displacement profiles for the five BBMSE configurations and the single isolated wall are more or less similar across the majority of the wall height. There are only minor and gradual differences observed between configurations. The W/H = infinite (single isolated wall), W/H = 3.0, W/H = 2.0, W/H = 1.7, and W/H = 1.4 configurations produce displacement profiles that are nearly coincident throughout the full wall height. There are differences between adjacent profiles of less than 0.3 mm at most elevations. This close agreement among these five configurations suggests that, for W/H ratios of 1.4 and above, the inter-wall spacing has a negligible influence on the lateral wall displacement under self-weight loading. And the two opposing walls in these configurations behave essentially as independent structures in terms of their facing deformation response.

The W/H = 1.2 configuration is the clear exception to this pattern that exhibits a noticeably lower lateral displacement than all other configurations across the full wall height. The maximum lateral displacement for the W/H = 1.2 configuration is approximately 4.6 mm at H ≈ 3.1 m, compared with approximately 5.2 mm for all other configurations at the same elevation. It shows an increase of approximately 10% relative to the single isolated wall reference case.

Physical Interpretation of W/H = 1.2 Behavior:

The reduced lateral displacement observed for the W/H = 1.2 configuration relative to all other configurations under self-weight loading is attributed to the overlap of the reinforced fill zones of the two opposing walls at this spacing. At W/H = 1.2, the inter-wall spacing of W = 7.2 m is sufficiently small relative to the reinforcement length that the reinforcement layers of the two opposing walls extend into. It potentially overlaps within the shared fill zone and creates a condition in which the stress fields of the two walls interact directly.

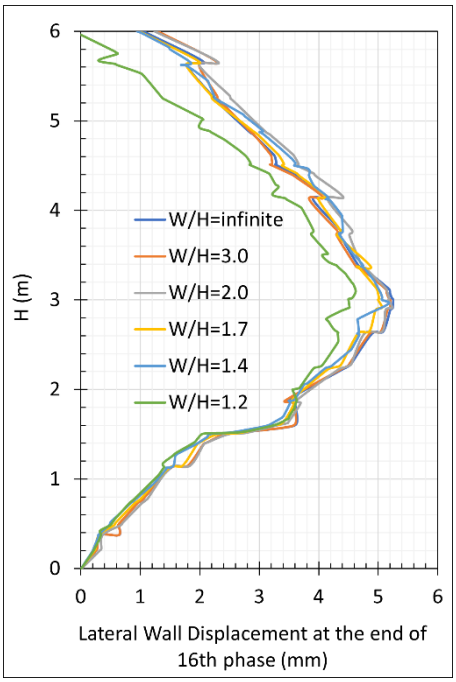

Figure 4.4: Lateral wall displacement profiles BBMSE wall configurations

The behavior of the W/H = 1.2 configuration therefore represents a distinct behavioral regime the overlapping interaction regime in which the reinforcement layers of the two opposing walls share a common fill zone thus producing structural responses that differ qualitatively from those of the non-overlapping configurations (W/H = 1.4 to 3.0). Here the opposing reinforcement layers are separated and the walls interact only through the stress field of the shared fill rather than through direct reinforcement overlap.

4.3.2 Lateral earth pressure behind the reinforcement zone

General Distribution Pattern

Figure 4.5 shows that all three numerically predicted lateral earth pressure profiles exhibit a broadly linear increase with depth from zero at the wall crest to a maximum

value at the base of the wall. It is broadly consistent with the classical triangular earth pressure distribution expected for a cohesionless granular fill under static loading conditions. The profiles start at approximately zero pressure at H = 6.0 m at the wall crest and increase progressively with decreasing elevation. It reaches their respective maximum values at the base of the wall at H = 0. This linear depth-dependent pattern verifies that the primary driver of lateral earth pressure behind the reinforcement zone is the increasing overburden stress with depth. It is consistent with the Rankine active earth pressure framework adopted in the FHWA simplified design method for MSE wall external stability design.

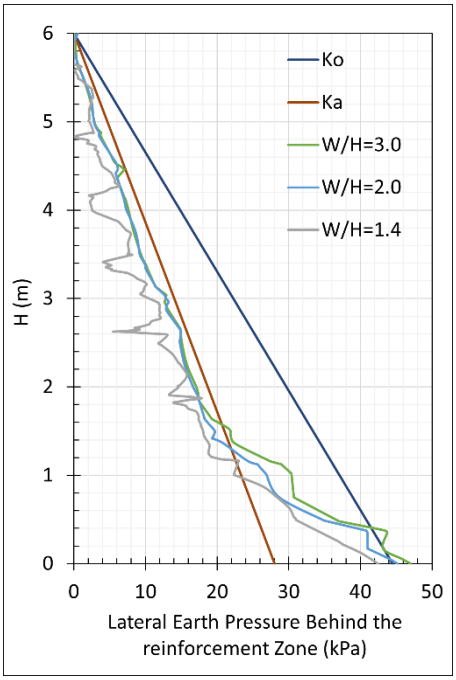

Figure 4.5: Lateral earth pressure distribution behind the reinforcement zone.

The lateral earth pressure distribution behind the reinforcement zone exhibits a clear transition with depth. Above approximately 1.5 m from the base, the computed pressures closely approach the active earth pressure condition. Below this depth, they tend toward the at-rest state. This behavior can be attributed to the boundary and facing conditions adopted in the model. The upper portion of the wall incorporates elastomeric bearing pads modeled as freely rotating hinges. It which permit rotational flexibility and lateral deformation of the facing. This flexibility enables sufficient wall movement to mobilize active earth pressure conditions in the upper zone. In contrast, the lower approximately 1.5 m of the wall is effectively restrained due to fixity at the base which limits lateral displacement and preventing full mobilization of active

conditions. Consequently, the soil in this region remains closer to an at-rest state, consistent with Rankine's earth pressure theory.

Influence of W/H Ratio on Lateral Earth Pressure

The important finding from above figure is consistent reduction in lateral earth pressure behind the reinforcement zone with decreasing W/H ratio. The W/H = 3.0 configuration exhibits the highest lateral earth pressure among the three BBMSE configurations. There is a maximum pressure at the base of the wall of approximately 46 kPa. The W/H = 2.0 configuration exhibits a slightly lower maximum pressure of approximately 44 kPa at the base. It represents a minor reduction relative to W/H = 3.0. The W/H = 1.4 configuration exhibits the most significant reduction, with a maximum pressure at the base of approximately 40 kPa a reduction of approximately 14% relative to the W/H = 3.0 configuration.

This progressive reduction in lateral earth pressure with decreasing W/H ratio is directly attributable to the interaction between the reinforced fill zones of the two opposing walls as the inter-wall spacing decreases. As the spacing between the two wall facings reduces, the reinforcement layers of the opposing walls increasingly encroach upon the shared fill zone. It constrains the lateral deformation of the fill between the two walls and thus preventing the full development of the active failure wedge behind each wall. This suppression of the active failure wedge identified analytically by Han & Leshchinsky (2010) as occurring at W/H ratios of 2 to 3 reduces the lateral earth pressure behind the reinforcement zone below the value that would develop in a single isolated wall under the same loading conditions because the constrained fill zone cannot mobilize the full active state associated with unrestricted lateral yield.

The reduction in lateral earth pressure is observed to be gradual and progressive rather than exhibiting a sharp threshold at a specific W/H ratio. The pressure reduction occurs as the W/H ratio decreases from 3.0 to 1.4. The absence of a sharp threshold in the earth pressure response confirms that BBMSE wall interaction is a continuously evolving phenomenon rather than a binary condition that switches on or off at a specific W/H ratio.

4.3.3 Lateral earth pressure at the wall facing

General Distribution Pattern

The lateral earth pressure distributions at the wall facing shown in Figure 4.6 differ from the lateral earth pressure distributions behind the reinforcement zone presented previously. It differs in two important respects. First, the magnitudes of the pressures at the wall facing are substantially lower than those behind the reinforcement zone at corresponding depths. It shows the significant reduction in lateral stress that occurs within the reinforced fill zone as the earth pressure is transferred from the retained fill through the reinforcement elements to the facing.

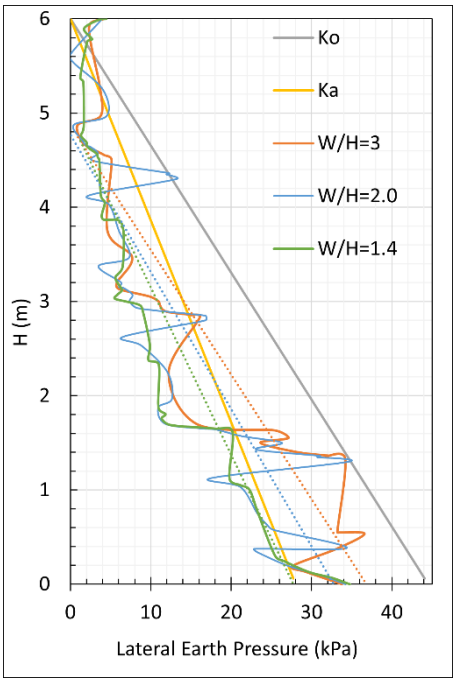

Figure 4.6: Lateral earth pressure distribution at the wall facing

Second, the profiles at the wall facing exhibit pronounced oscillations and local variations with depth that are far more irregular and complex than the relatively smooth triangular profiles observed behind the reinforcement zone. It shows the discrete nature of the reinforcement-facing connection system and the local stress redistribution associated with each panel connection point and reinforcement layer level. These complex pressure distributions at the facing are a direct consequence of the flexible jointed facing system of the reference wall. It comprises precast concrete panels connected through EPDM bearing pads modeled with zero rotational stiffness hinges which prevents the development of a continuous smooth pressure distribution. It instead produces a series of locally concentrated pressure zones at each reinforcement connection level.

Influence of W/H Ratio on Lateral Earth Pressure at the Facing

Consistent with the trend observed for the lateral earth pressure behind the reinforcement zone in previous section, the lateral earth pressure at the wall facing shows a progressive reduction with decreasing W/H ratio across all depths. The W/H = 3.0 exhibits the highest lateral earth pressures among the three BBMSE configurations at most depths. There are maximum pressure values reaching approximately 36 kPa in the lower portion of the wall near H = 0.5 m. The W/H = 2.0 configuration exhibits pressures broadly similar to W/H = 3.0 throughout most of the wall height. There slightly lower peak values in the lower portion of the wall. The W/H = 1.4 configuration exhibits the most consistently lower lateral earth pressures representing a reduction up to 28 kPa. It is approximately 20% relative to the W/H = 3.0 configuration at comparable depths.

This progressive reduction in facing pressure with decreasing W/H ratio is physically consistent with the reduction in horizontal earth pressure exerted on the back of reinforcement zone documented in previous section. It reflects the same underlying mechanism the suppression of the active failure wedge development within the constrained shared fill zone as the inter-wall spacing decreases. As the spacing reduces, the reinforced fill zones of the two opposing walls increasingly interact. The lateral earth pressure mobilized within the fill is progressively reduced, resulting in lower pressures transmitted to the facing panels through the reinforcement connection system.

4.3.4 T_{max} distribution under vehicle surcharge loading

General Distribution Pattern

All five BBMSE configurations exhibit a consistent and characteristic T_{max} distribution with depth under vehicle surcharge loading as shown in Figure 4.7. Here, the reinforcement tension is lower in the upper portion of the wall between H = 6.0 m and approximately H = 2.0 m. It increases progressively with decreasing elevation to reach a peak maximum value in the lower portion of the wall, at the second lowest reinforcement, before reducing slightly at the lower reinforcement layer. The flexible facing prevents the redistribution of reinforcement loads toward the upper connection points. It allows the classical overburden-driven concentration of peak tensions in the lower reinforcement layers to persist under the combined self-weight and vehicle surcharge loading condition.

Influence of W/H Ratio on T_{max}

The most important finding from the above figure is the reduction in T_{max} with decreasing W/H ratio under vehicle surcharge loading. It confirms that the inter-wall spacing interaction effect remains significant. The reduction in T_{max} with decreasing W/H ratio is observed consistently across all reinforcement levels.

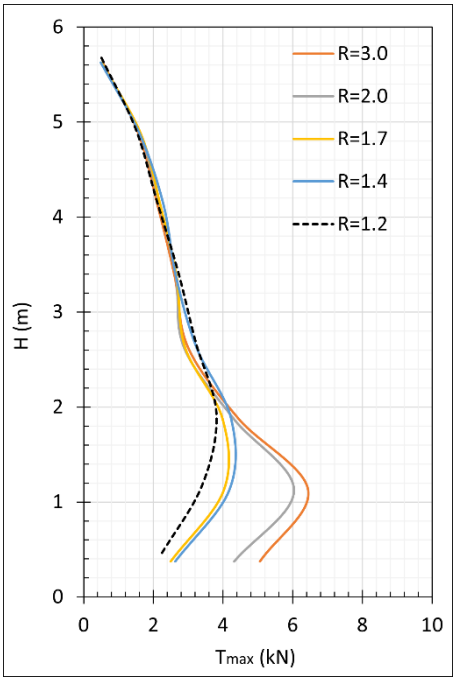

Figure 4.7: T_{max} distribution with depth at vehicle surcharge loading condition.

The W/H = 3.0 configuration exhibits the highest T_{max} values among the five configurations. A peak maximum tensile force of approximately 6.4 kN is seen at the second lowermost layer. The W/H = 2.0 configuration shows similar distribution to W/H = 3.0 throughout the upper and mid-height regions of the wall. A slightly lower peak T_{max} of approximately 6.0 kN at a comparable elevation is seen which represent a slight reduction of approximately 7% relative to W/H = 3.0. The close proximity of the W/H = 3.0 and W/H = 2.0 profiles observed consistently proves that these two configurations behave in a nearly identical manner. And that the inter-wall spacing interaction effect remains relatively minor for W/H ratios in the range of 2.0 to 3.0.

The W/H = 1.7 configuration exhibits a noticeably lower peak T_{max} of approximately 4.0 kN, representing a reduction of approximately 35% relative to W/H = 3.0. This more substantial reduction relative to W/H = 2.0 and W/H = 3.0 confirms that the W/H range between 1.7 and 2.0 represents an important transition zone in the

interaction behavior under vehicle loading below which the inter-wall spacing begins to have a substantially more pronounced effect on the reinforcement tensile forces.

The W/H = 1.4 configuration exhibits a peak T_{max} of approximately 4.0 kN, approximately similar to W/H = 1.7 value. The two curves run closely parallel. The similarity between the W/H = 1.4 and W/H = 1.7 T_{max} profiles suggests that the rate of T_{max} reduction with decreasing W/H ratio is slowing in this range. The interaction effect approaches a plateau below which further reductions in inter-wall spacing produce diminishing additional reductions in reinforcement tension. The W/H = 1.2 configuration exhibits the most significant reduction of all five configurations, with a peak T_{max} of 3.8 kN. It is a reduction of approximately 40% relative to the W/H = 3.0 peak value of approximately 6.4 kN. As observed under self-weight loading, with the curve bending back toward lower T_{max} values more sharply and at a higher elevation than the other four configurations. It results in a distinctly different profile shape in the lower wall region that is characteristic of the overlapping interaction regime in which the reinforcement layers of the two opposing walls share a common fill zone.

4.3.5 Critical failure surfaces pattern

Incremental deviatoric strain ($\Delta\gamma_s$) in PLAXIS serves as an indicator of shear localization. It provides a precise developing failure mechanism within an MSE wall. Contrary to displacement plots that show broad zones of movement, the deviatoric strain identifies the exact paths where soil grains are undergoing intense distortion that trace the nascent slip surfaces. In back-to-back wall configurations, these strain patterns reveal the transition from kinematic interaction to structural independence. At narrow width-to-height ratios, the shear bands intersect deep within the reinforced zone to form a unified, merged mechanism. As the ratio increases toward 2.0, these bands migrate toward the crest. It separates at a ratio of 3.0 into two distinct triangular wedges. This localization not only shows the extent of the active zone but also highlights the influence of reinforcement.

The strain bands often show shift where they cross geogrid layers, reflecting the transfer of shear stress and the effective pinning of the failure surface by the reinforcement. The incremental deviatoric strain distribution for the W/H = 1.2 and 1.4 configurations reveal a single combined failure mechanism acting across the full width of the wall system. The strain concentrations are distributed relatively uniformly across the entire reinforced fill zone. The absence of distinct localized shear bands at the back of either wall facing confirms that the two opposing walls are acting

as a single monolithic RE mass at this spacing. The failure mechanism is engaging the full combined width of the reinforced fill rather than developing independently within each wall.

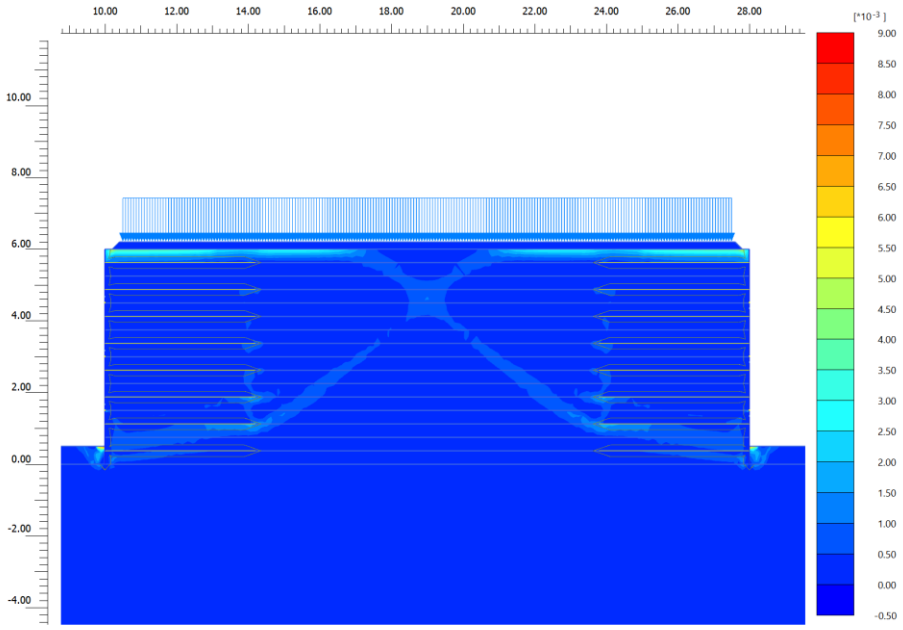

(a) W/H=3.0

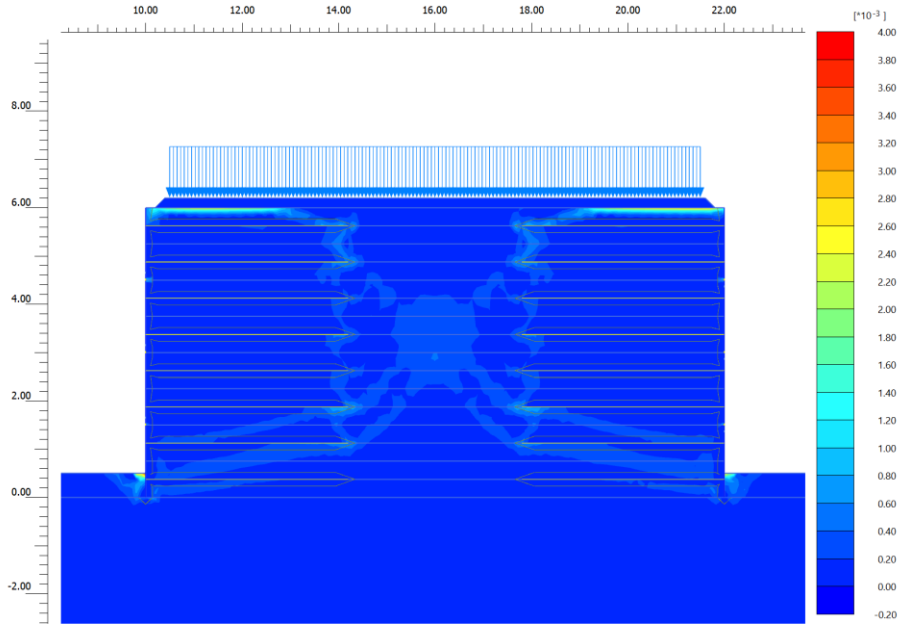

(b) W/H=2.0

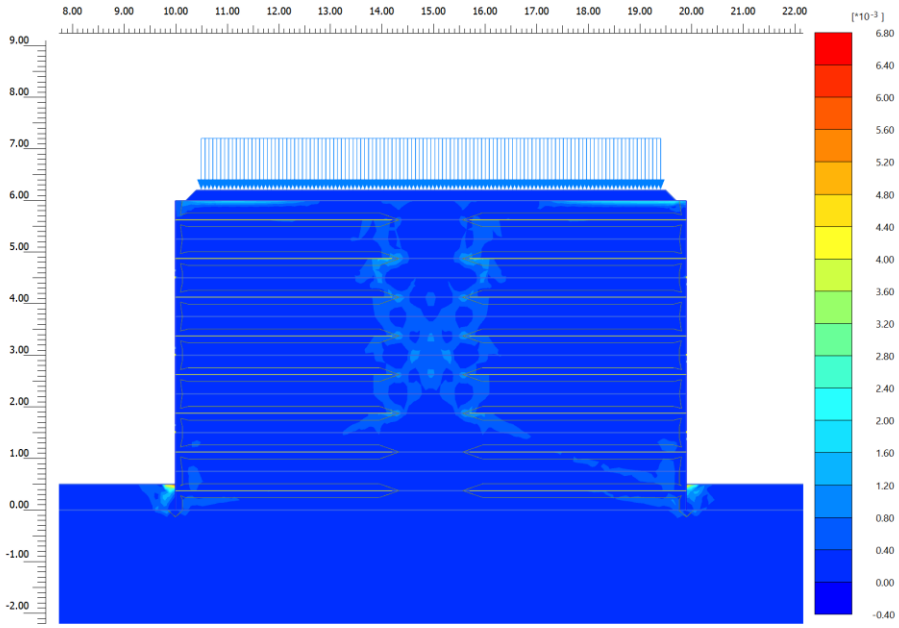
8.00 9.00 10.00 11.00 12.00 13.00 14.00 15.00 16.00 17.00 18.00 19.00 20.00 21.00 22.00
9.00 8.00 7.00 6.00 5.00 4.00 3.00 2.00 1.00 0.00 -1.00 -2.00
[*10-3]
6.80 6.40 6.00 5.60 5.20 4.80 4.40 4.00 3.60 3.20 2.80 2.40 2.00 1.60 1.20 0.80 0.40 0.00 -0.40

(c) W/H=1.7

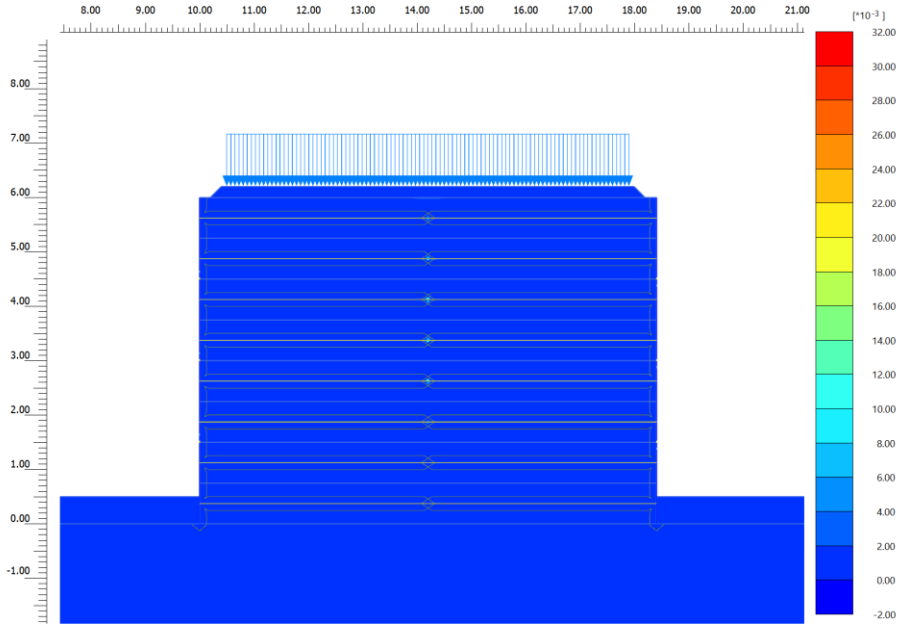
8.00 9.00 10.00 11.00 12.00 13.00 14.00 15.00 16.00 17.00 18.00 19.00 20.00 21.00
8.00 7.00 6.00 5.00 4.00 3.00 2.00 1.00 0.00 -1.00
[*10-3]
32.00 30.00 28.00 26.00 24.00 22.00 20.00 18.00 16.00 14.00 12.00 10.00 8.00 6.00 4.00 2.00 0.00 -2.00

(d) W/H=1.4

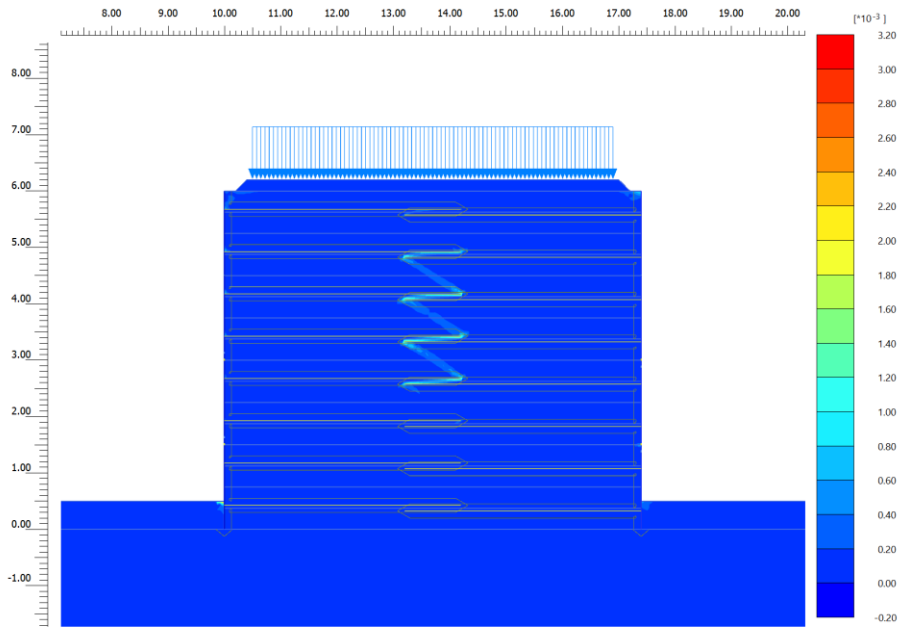

(e) W/H=1.2

Figure 4.8: $\Delta\gamma_s$ distributions from the phi-c reduction analysis in stage 19

The incremental deviatoric strain distribution for the W/H = 1.7 configuration marks a critical transition in the failure mechanism pattern showing for the first time a clearly noticeable structure. Here, two partially independent failure wedges are beginning to develop one associated with each opposing wall while still interacting through the central fill zone between them. The oval-shaped strain concentrations at the reinforcement tips visible in above figure correspond directly to the points at which the potential failure surface would emerge from the end of each reinforcement layer. Their connection through the central fill zone verifies that the failure mechanism at W/H = 1.7 is neither fully combined as at W/H = 1.2 and 1.4 nor fully independent as would be expected for non-interacting walls. But it is rather a transitional mechanism in which the failure wedges of the two opposing walls are geometrically linked through their shared central fill zone.

This transitional failure mechanism at W/H = 1.7 is directly consistent with the T_{max} analysis. It identified the W/H range of 1.7 to 2.0 as the critical transition zone between the interacting and near-independent behavioral regimes. It also provided visual confirmation from the failure surface geometry that this spacing represents the start of a qualitatively different structural behavior relative to the more closely spaced configurations.

The incremental deviatoric strain distribution for the W/H = 2.0 configuration shows a further evolution of the failure mechanism toward two more clearly distinct and partially independent failure wedges. It is developing behind each wall facing. Compared with W/H = 1.7, the two strain concentration zones associated with the reinforcement tips of the opposing walls at W/H = 2.0 are more spatially separated. The connecting strain field in the central fill zone is less intense which indicates that the two failure wedges are beginning to decouple from each other with the increase in spacing. But the failure mechanism is not yet fully independent. The strain concentrations at the reinforcement tips of the two opposing walls still overlap to some degree in the central fill zone that confirms that W/H = 2.0 remains within the transitional to weakly interacting behavioral regime.

The incremental deviatoric strain distribution for the W/H = 3.0 configuration represents the stage of the progression toward independent wall behavior. It shows two clearly distinct and largely independent failure mechanisms. One is associated with each opposing wall. There is minimal interaction between them through the central fill zone. The strain concentration pattern shows well-defined and spatially separated shear zones which develops behind each wall facing. The highest strain intensities are concentrated near the outer corners of each wall at the base. And it extends diagonally upward and inward through the reinforced fill zone. This is in a pattern broadly consistent with the classical active failure wedge geometry.

The two failure mechanisms at W/H = 3.0 are oriented symmetrically about the centerline of the BBMSE system. Here, each mechanism develops independently within the reinforced fill zone of its respective wall. The central fill zone between the two failure mechanisms shows relatively low strain concentrations. It confirms that the two opposing walls are behaving as essentially independent structures in terms of their failure mechanism at this spacing.

The incremental deviatoric strain plots for the five BBMSE wall configurations collectively reveal a clear and systematic progressive evolution of the failure mechanism. With increasing W/H ratio, transitioning from a fully combined mass failure at W/H = 1.2 to two independent failure wedges at W/H = 3.0 is seen through a series of well-defined intermediate stages. This progressive evolution entirely consistent with the structural response trends identified in the preceding sections. The transition from combined to independent failure mechanisms provides direct

visual confirmation of the interaction distance assessment which was presented in the preceding sections.

4.3.6 Plastic points distribution at end of construction stage 16

The plastic points locate the stress state reaching MC yield surface within the FE mesh, indicating that the soil at those points is in a state of active plastic deformation rather than elastic response. Therefore, the distribution of plastic points provides a visual observation of the zones of yielded soil within the reinforced fill zone and foundation, complementing the incremental strain distributions by identifying the pattern of plasticity mobilized and spatial extent under self-weight loading.

The plastic point distributions at the end of Stage 16 collectively shows a systematic and physically consistent progressive evolution in the spatial extent and pattern of soil plasticity with increasing W/H ratio, transitioning from a fully yielded monolithic fill mass at W/H = 1.2, in which virtually the entire fill is in plastic failure through increasingly structured patterns with growing central elastic cores at W/H = 1.4, 1.7, and 2.0, to two fully separated lateral plastic zones with a fully elastic central core at W/H = 3.0.

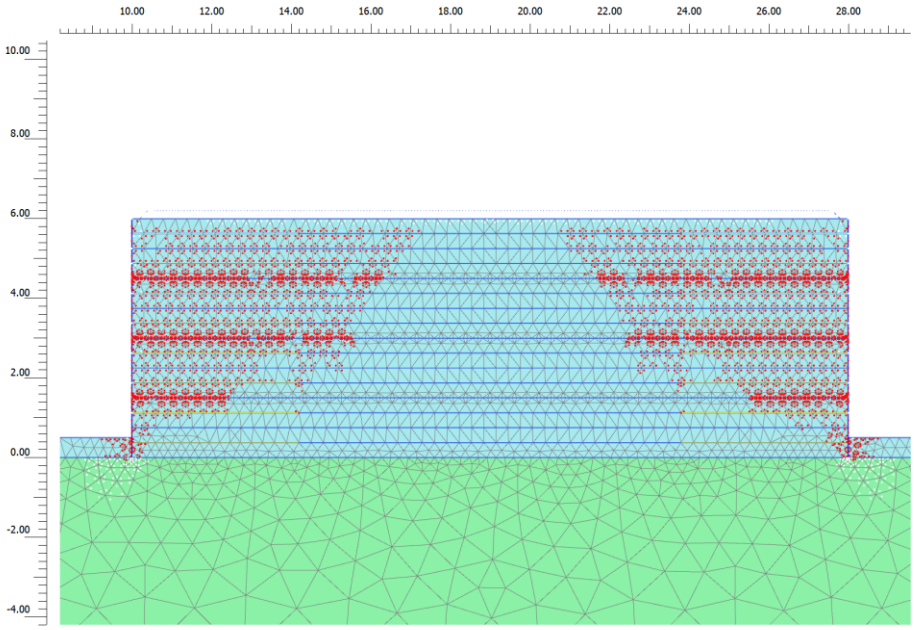

(a) W/H=3.0

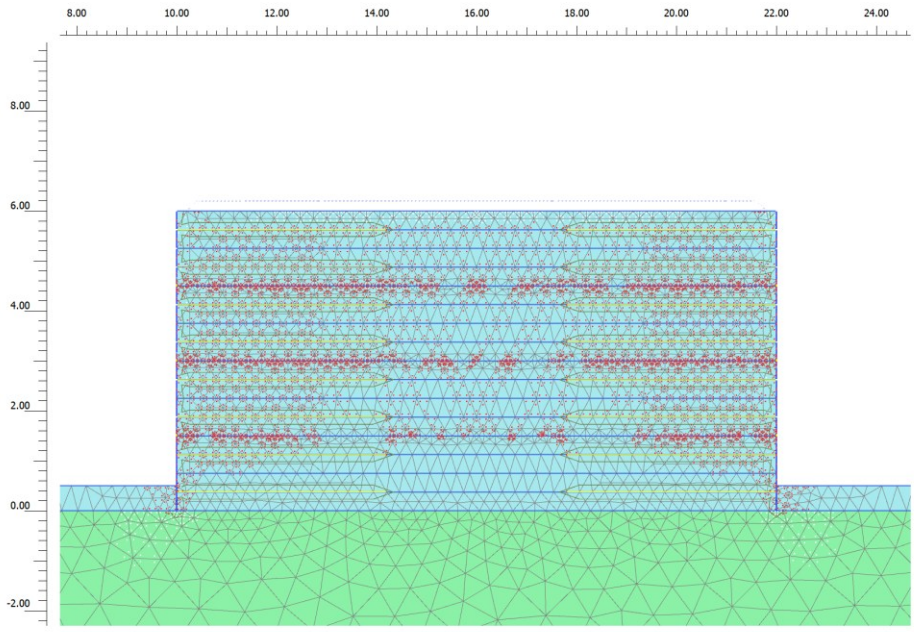
8.00
10.00
12.00
14.00
16.00
18.00
20.00
22.00
24.00
8.00
6.00
4.00
2.00
0.00
-2.00

(b) W/H=2.0

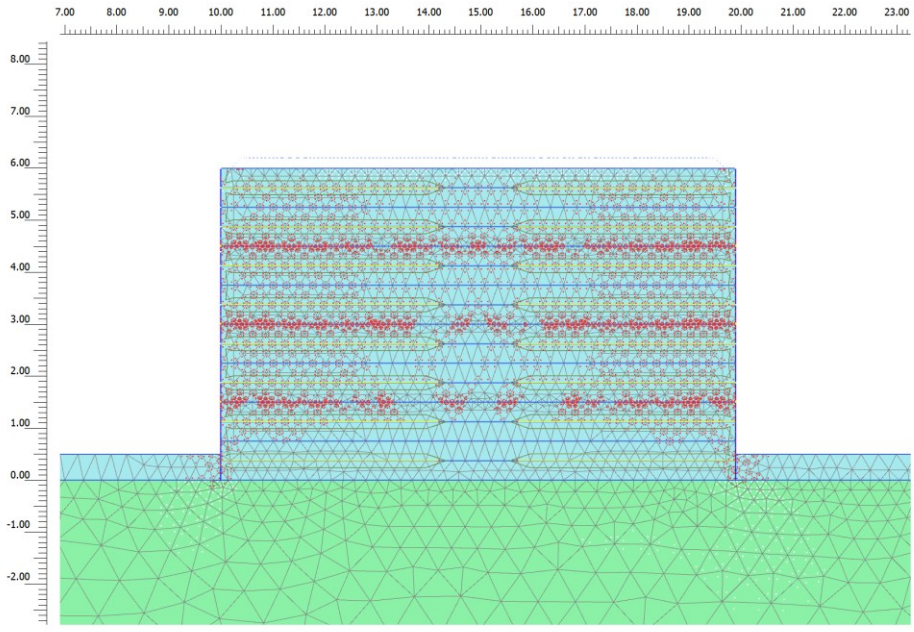
7.00
8.00
9.00
10.00
11.00
12.00
13.00
14.00
15.00
16.00
17.00
18.00
19.00
20.00
21.00
22.00
23.00
8.00
7.00
6.00
5.00
4.00
3.00
2.00
1.00
0.00
-1.00
-2.00

(c) W/H=1.7

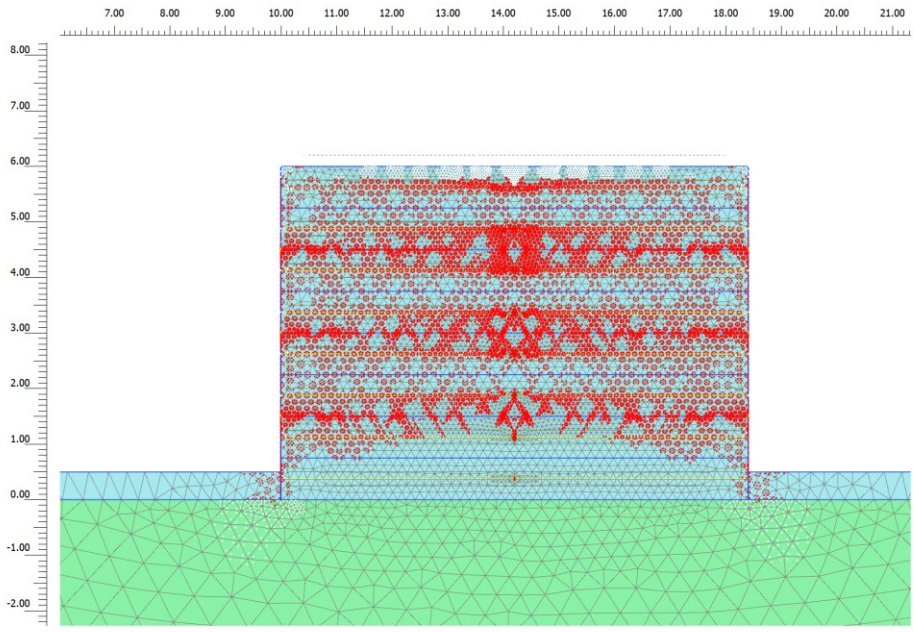

(d) W/H= 1.4

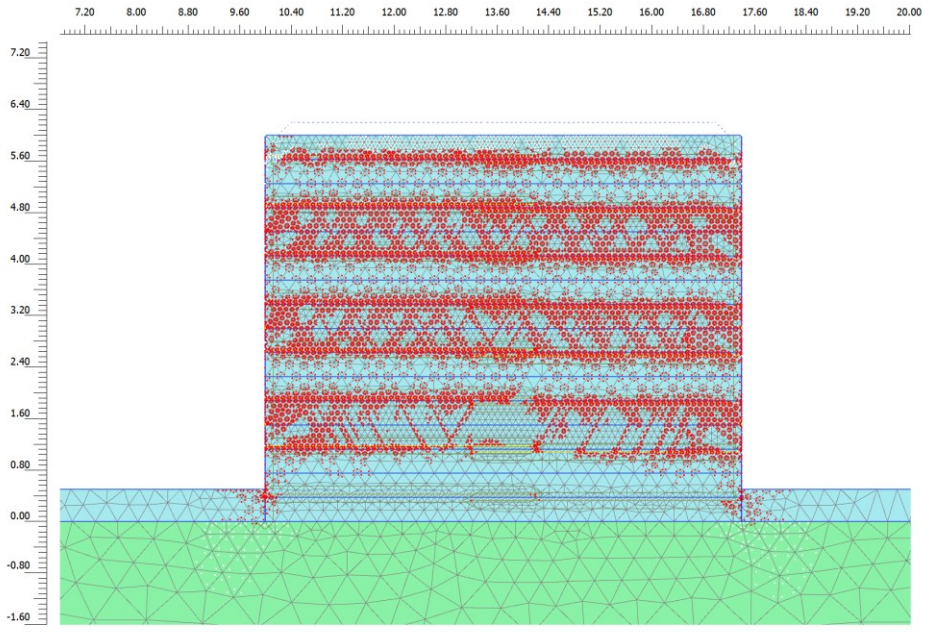

(e) W/H= 1.2

Figure 4.9: Plastic points distribution at end of construction stage 16

4.3.7 Incremental displacement distribution at limit state

To identify the precise cause of failure of an MSE wall, the PLAXIS feature of incremental displacement plots is used to isolate the movements that take place

during the current calculation step and not the previous cumulative history of the movement. It specifies the critical failure surface that could appear as a concentrated shear band in a phi-c reduction phase that allow to distinguish between failure modes. The process can be referred to as global instability (deep-seated arcs), base sliding, or wall bulging as a result of overstress of reinforcement through such displacement shadings shape and direction.

These visualizations can be compared with theoretical models. Whether the angle of failure is in agreement with Rankine or Coulomb theory or whether the soil is moving over the geogrids in a pull-out failure can be known. The incremental displacement patterns across the varying W/H ratios as shown in Figure 4.10. gives understanding of a clear transition from a fully coupled structural system to independent wall system. At a ratio of 1.2, the failure surfaces from both faces overlap, creating a unified mass that encompasses the entire width of the backfill. As the ratio increases through 1.4 and 1.7, the intersection of these slip surfaces migrates toward upper region, forming a distinct "V" shape and indicating a reduction in interaction scale. As the ratio reaches 2.0, the walls reach a condition where the failure wedges touch at the crest. And at a ratio of 3.0, the mechanisms become nearly independent, separated by a central zone of negligible displacement. This progression shows that as the distance between wall faces increases, the silo effect dissipates which allows each reinforced mass to develop its own failure wedge without interference from the opposing side.

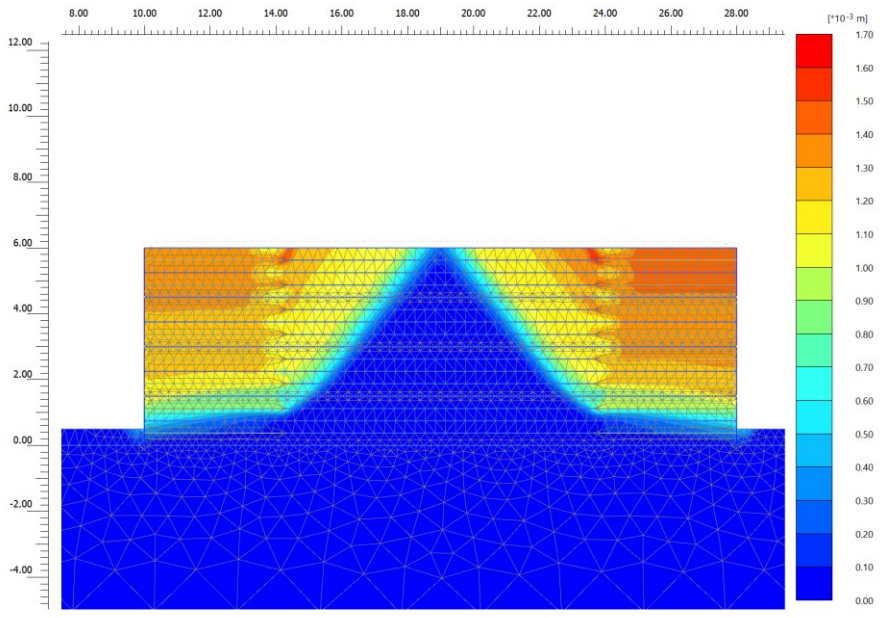

(a) W/H= 3.0

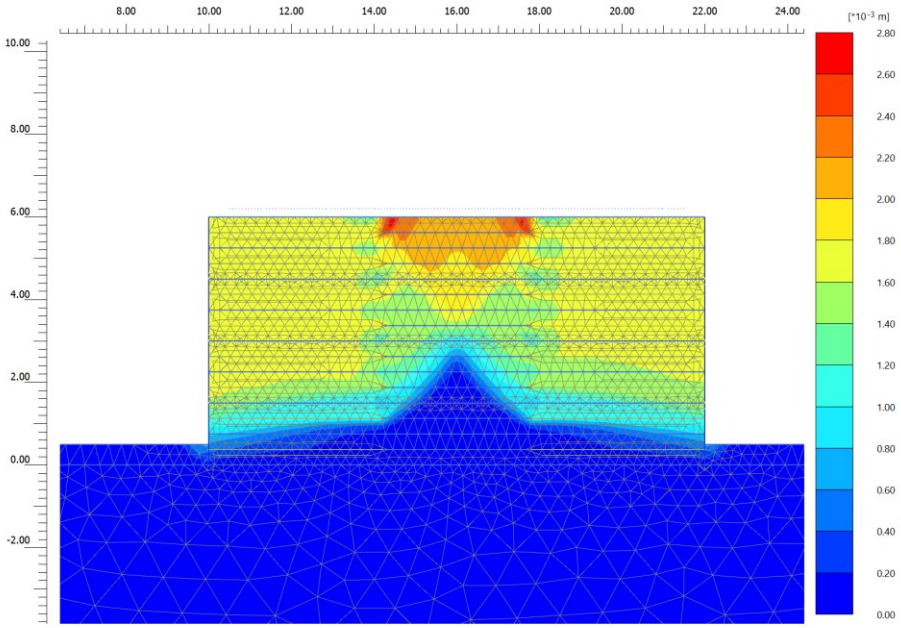
8.00
10.00
12.00
14.00
16.00
18.00
20.00
22.00
24.00
[*10-3 m]
10.00
8.00
6.00
4.00
2.00
0.00
-2.00
2.80
2.60
2.40
2.20
2.00
1.80
1.60
1.40
1.20
1.00
0.80
0.60
0.40
0.20
0.00

(b) W/H= 2.0

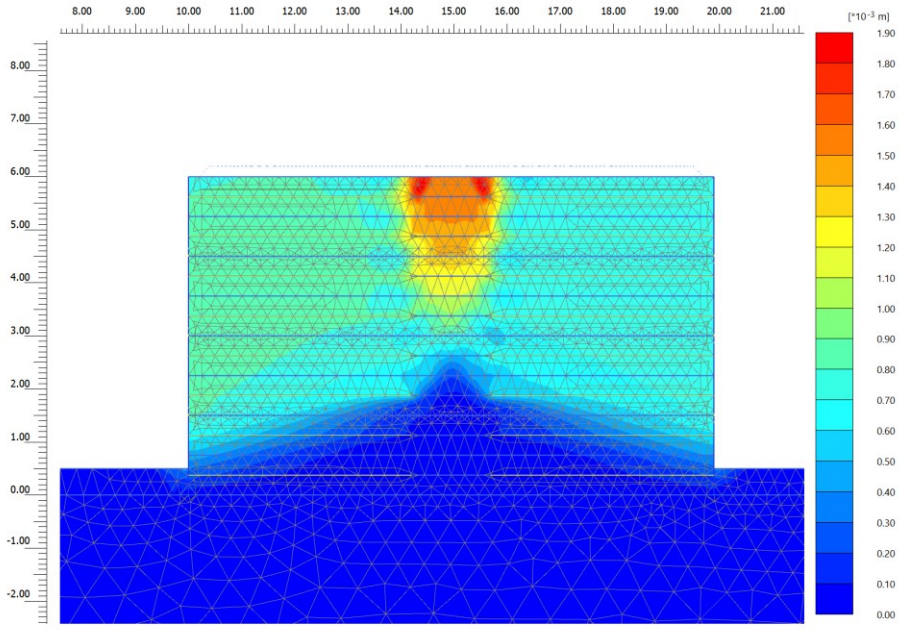
8.00
9.00
10.00
11.00
12.00
13.00
14.00
15.00
16.00
17.00
18.00
19.00
20.00
21.00
[*10-3 m]
8.00
7.00
6.00
5.00
4.00
3.00
2.00
1.00
0.00
-1.00
-2.00
1.90
1.80
1.70
1.60
1.50
1.40
1.30
1.20
1.10
1.00
0.90
0.80
0.70
0.60
0.50
0.40
0.30
0.20
0.10
0.00

(c) W/H= 1.7

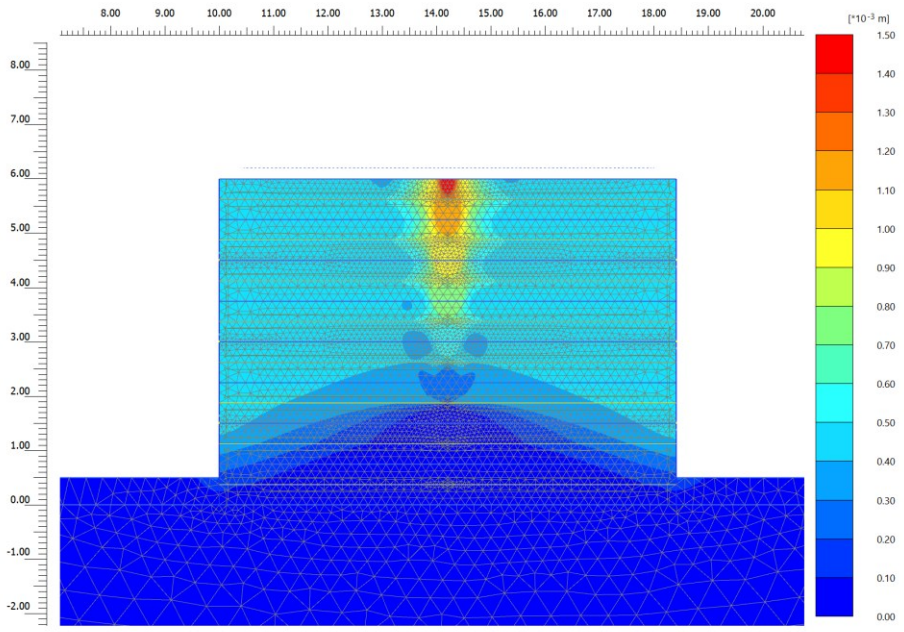

(d) W/H= 1.4

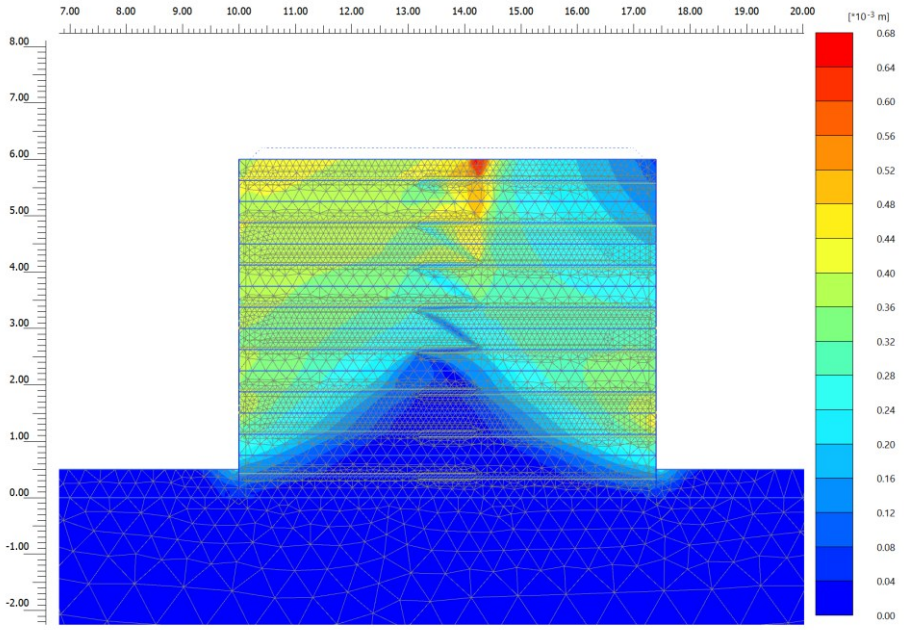

(e) W/H= 1.2

Figure 4.10: Incremental displacement distribution at limit state at stage 16

It should be noted that these incremental displacement plots should be interpreted qualitatively rather than quantitatively. In a Safety analysis (Phi-c reduction), PLAXIS

is not calculating actual physical deformations that would occur under service loads; instead, it is mathematically forcing the system toward collapse by reducing the soil's strength parameters. The absolute values do not represent actual displacement but is a way to identify which zones are moving more, relative to others. These figures show the existence and location of the failure surface.

4.4 Effect of Reinforcement Connectivity

A significant practical consideration in the design and construction of BBMSE wall systems is whether the reinforcement layers of the two opposing walls are physically connected at their tips or not. This distinction has implications for the structural behavior of the BBMSE system. The connected reinforcement creates a direct mechanical link between the two opposing walls through the central fill zone, potentially modifying the lateral earth pressure, reinforcement tension distribution, and wall facing deformation relative to the unconnected case.

4.4.1 Axial force distribution in reinforcement

The axial force distribution in the connected reinforcement system displays a broadly uniform and symmetric distribution of tensile forces along each reinforcement layer throughout the full wall height as shown in F*igure* 4.11. The force distribution along each reinforcement layer shows a characteristic pattern in which the tension is relatively high near both facing connection ends and exhibits a gentle dip toward the center of the span consistent with the mobilization of tensile resistance at both ends of the connected reinforcement element as it is pulled outward by the lateral earth pressure from both opposing walls simultaneously. This symmetric double-peak tension pattern along the reinforcement length is a direct consequence of the mechanical continuity between the two opposing walls through the connected reinforcement, which creates a system in which each half of the reinforcement element behaves analogously to an independent MSE wall reinforcement strip anchored at the central connection point rather than terminating freely in the fill.

The axial force distribution in the unconnected reinforcement system displays a markedly different pattern. The force distribution along each reinforcement layer shows a pattern in which the tension is highest near the facing connection and decreases progressively toward the free tip of the reinforcement in the central fill zone, reaching near-zero values at the reinforcement tip. This pattern is consistent with the standard MSE wall pullout mechanism in which tension is mobilized near the

facing and transferred to the surrounding fill through interface friction along the reinforcement length, without any mechanical continuity to the opposing wall's reinforcement system.

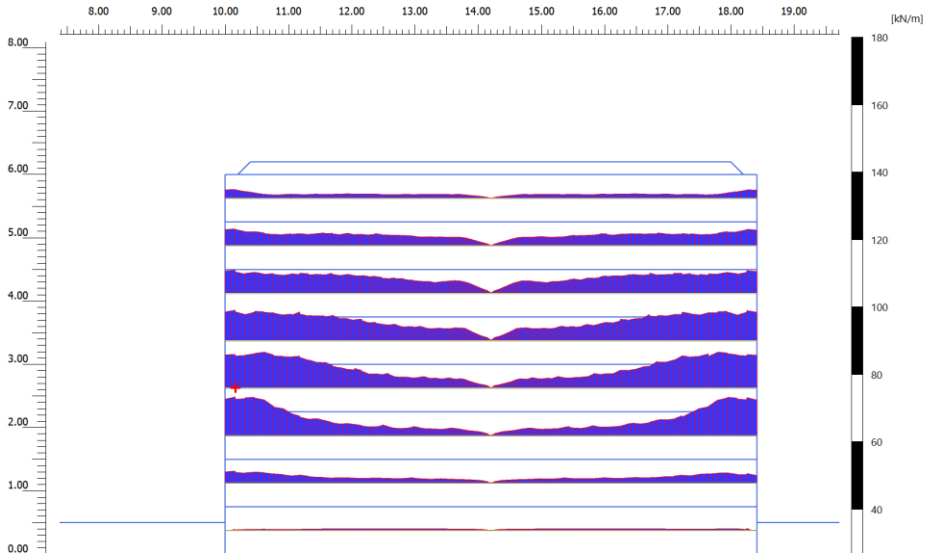

(a) Connected case

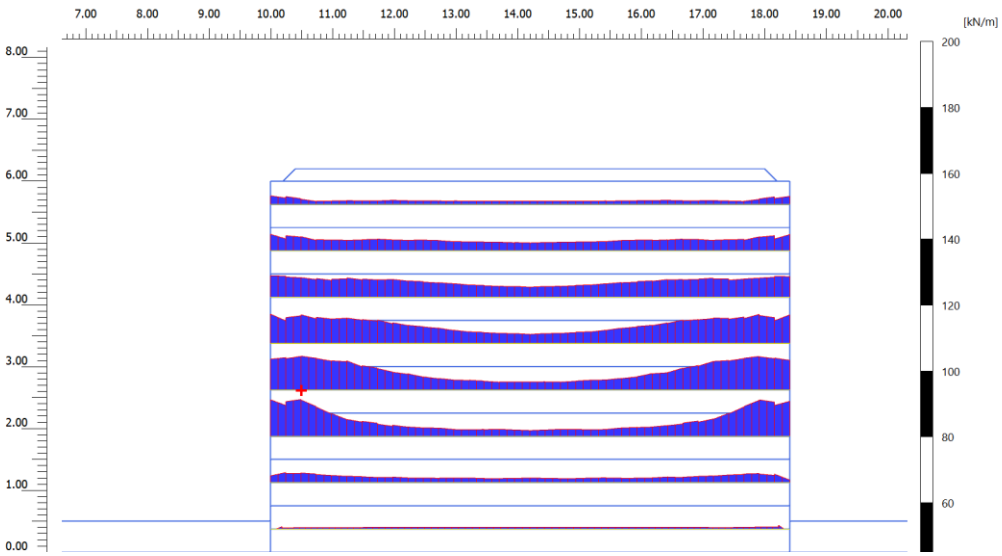

(b) Unconnected case

F*igure 4.11: Tension distribution at the working state*

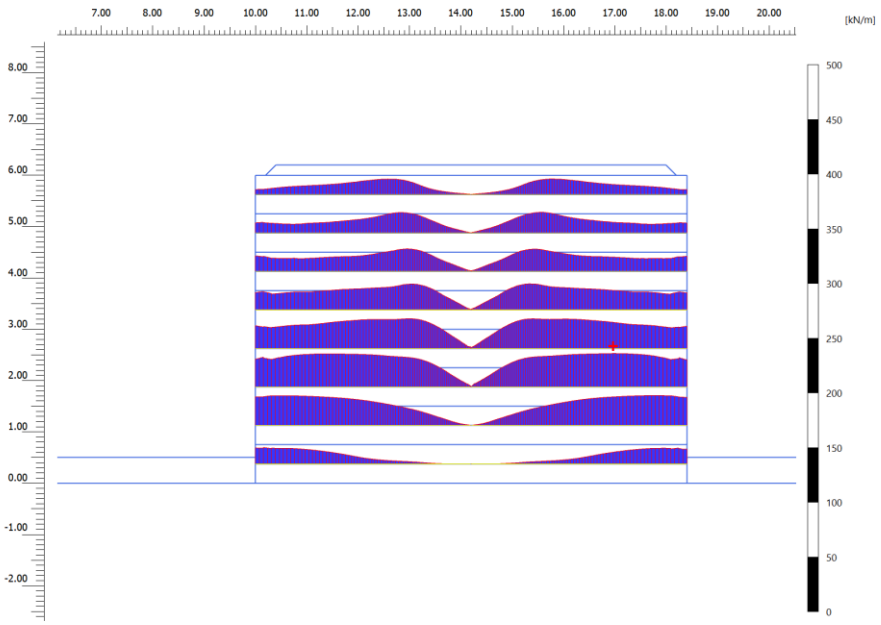

(a) Unconnected case

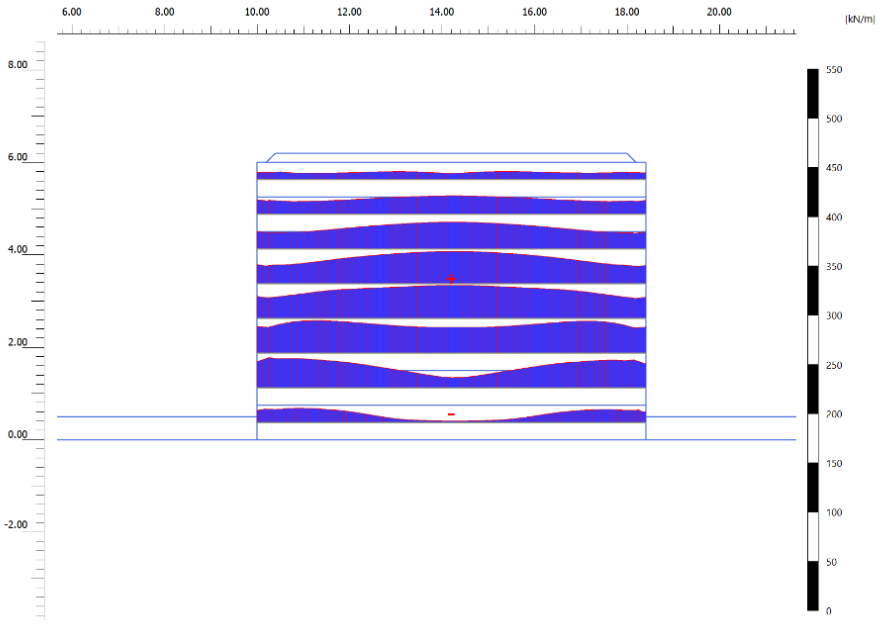

(b) Connected case

Figure 4.12: Tension distribution at the limit state

The uniform and symmetric nature of the axial force distribution at the FOS phase in the connected case indicates that even the central span of each reinforcement element carries a non-negligible tensile force confirms that the connected reinforcement is

fully engaged across its entire length at the limit state, with no portion of the reinforcement experiencing zero tension. This uniformity shows the ability of the connected system to distribute the forces evenly across the full reinforcement length compared to the unconnected case.

4.4.2 Lateral wall displacement

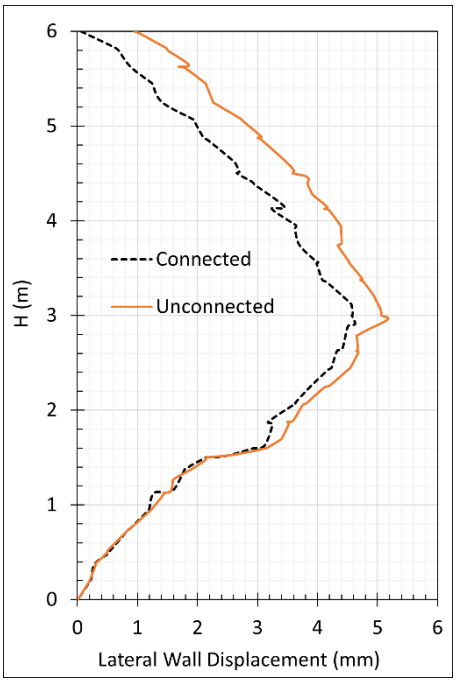

Figure 4.13: Lateral wall displacement profiles

A significant difference is observed between the two cases in terms of the magnitude of the lateral displacement throughout the wall height as shown in Figure 4.13. The unconnected case exhibits a higher maximum lateral displacement of approximately 5.2 mm occurring at approximately H = 3.0 m. The connected case exhibits a notably lower maximum lateral displacement of approximately 4.6 mm at a similar elevation, representing a reduction of approximately 12% relative to the unconnected case.

In the lower portion of the wall the connected and unconnected displacement profiles are nearly coincident indicating that the connectivity of the reinforcement has a negligible influence on the lateral displacement in the lower wall region where the overburden stress is high and the reinforcement provides effective confinement regardless of the connection condition. It is important to note that the lateral wall displacement at the crest level is nearly zero.

The reduction in lateral wall displacement in the connected case is attributed to the additional lateral restraint provided by the continuous connected reinforcement element, which directly links the two opposing wall facings through the shared fill zone and resists the outward lateral movement of each facing by mobilizing tension in the full span of the connected reinforcement simultaneously. This additional restraint effectively reduces the net lateral deformation of each wall facing relative to the unconnected case, where each wall's reinforcement acts independently without mechanical continuity to the opposing wall. This finding demonstrates that the connectivity of reinforcement layers across the shared fill zone in a BBMSE system can provide a meaningful serviceability benefit in terms of reduced facing deformation for closely spaced configurations.

4.4.3 Maximum reinforcement tensile force (T_{max})

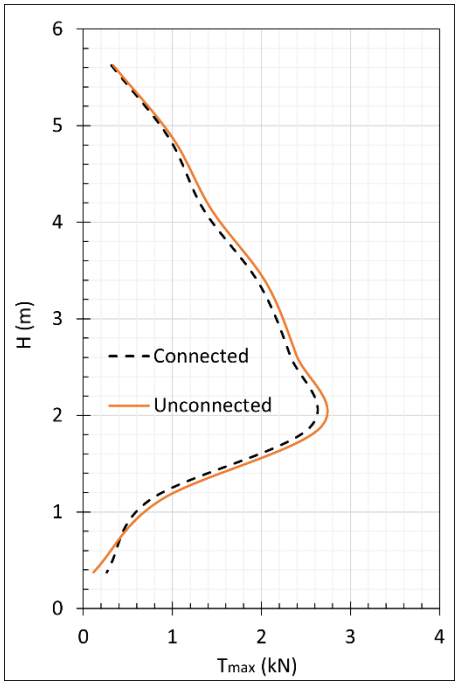

Figure 4.14: T_{max} distribution at the end of stage 16

The most significant observation from above figure is that the T_{max} values are remarkably similar between the connected and unconnected cases throughout the full wall height, with the two curves running closely parallel from the wall crest to the lower reinforcement levels as shown in Figure 4.14. The near-identical T_{max} values between the connected and unconnected cases despite the significantly different axial force distributions along the reinforcement length reflects the fact that the T_{max} represents the peak tensile force at the facing connection point which is governed

primarily by the lateral earth pressure acting on the facing panel at each reinforcement level rather than the total tensile load carried by the full reinforcement span.

This finding has important practical implications for reinforcement design: while the peak connection tension (T_{max}) is insensitive to the reinforcement connectivity condition and can be used to design the facing-reinforcement connection hardware regardless of whether the reinforcement is connected or unconnected across the fill zone, the total tensile load carried by the reinforcement which determines the required reinforcement tensile strength and the pullout demand along the full reinforcement length, is significantly higher in the connected case and must be accounted for in the reinforcement selection and anchorage design.

4.4.4 Lateral earth pressure at wall facing

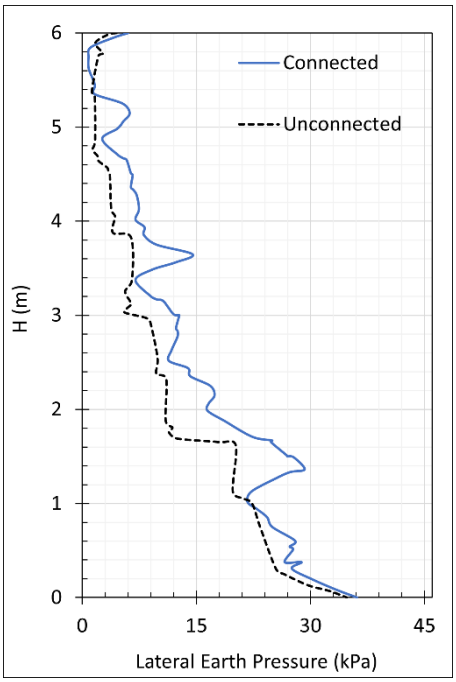

Figure 4.15: Lateral earth pressure distributions at the wall facing

The connected case exhibits higher lateral earth pressures than the unconnected case throughout the upper and mid-height regions of the wall as shown in Figure *4.15*. The higher lateral earth pressure at the facing in the connected case relative to the unconnected case in the upper and mid-height regions is physically explained by the additional lateral constraint imposed by the connected reinforcement on the fill between the two walls. In the connected case, the continuous reinforcement spanning

the full width of the BBMSE system prevents the central fill from moving laterally, effectively increasing the confining stress within the fill and consequently increasing the lateral earth pressure transmitted to the facing panels.

The most significant practical conclusion from this comparative analysis is that while the reinforcement connectivity does not alter the peak facing connection tension (T_{max}), which is the primary internal stability design parameter, it does have significant implications for the total reinforcement load, the lateral wall displacement, and the distribution of lateral earth pressure at the facing. Specifically, connected reinforcement reduces the lateral wall displacement, providing a serviceability benefit but increases the lateral earth pressure, increasing the structural demand on the facing panels. These findings show the importance of considering the reinforcement connectivity condition in the design of BBMSE wall systems for closely spaced configurations where the reinforcement layers of the two opposing walls are in proximity within the shared fill zone.

5 CONCLUSIONS AND RECOMMENDATIONS

5.1 Conclusions

This chapter concise the conclusions obtained from the comprehensive numerical investigation of BBMSE wall behavior under static vehicle loading conditions using PLAXIS 2D finite element software. The study was conducted in two principal stages, a model validation stage against the real-world field monitoring data of (Cristelo et al., 2016) for the Portuguese Highway A4 MSE wall, and a static parametric investigation stage examining the influence of inter-wall spacing-to-height ratio (W/H) on the structural performance of a standardized 6 m BBMSE wall under combined self-weight and static vehicle surcharge loading.

The validated PLAXIS 2D FEM model for BBMSE walls using real-world field data from Cristelo et al. (2016) showed good agreement in terms of wall displacement, peak reinforcement tension, and their distance from the point of connection. This established physical credibility of the furhter study. The analysis also revealed that conventional AASHTO-based failure surface assumptions tend to overestimate the location of peak reinforcement tension above certain height showing that classical design approaches fail to capture sufficienctly the behavior of MSE walls.

It is verified in the parametric analysis that the spacing-to-height ratio (W/H) dictates BBMSE interaction behavior. For W/H ≥ 2.0, walls tend to behave nearly independently, while W/H = 1.7–2.0 represents a critical transition zone. Below this range strong interaction occurs resulting to distinct deformation patterns and reduced reinforcement tensions. Earth pressure distributions were found to lie just below the active at the region where the panels are free to rotate due to hinged connection and approaches at-rest states when supported by the rigid support.

The study also showed that reinforcement connectivity has significantly improves serviceability performance, reducing displacement, maintaining peak forces but at a cost of increased lateral pressure. Evaluation of current design guidelines showed that the FHWA method is conservative for closely spaced walls and its geometric interaction criterion is too simplistic to identify the true critical spacing. Additionally, the research provides a more pragmatic threshold criterion (W/H ≈ 2.0) which highlights the certain limitations of existing design methods. Hence, it provides a physically validated framework for more accurate and efficient BBMSE wall design under highway loading conditions.

5.2 Recommendations

The study recommends adopting a critical interaction threshold of W/H ≈ 2.0 for BBMSE wall design under static vehicle loading. Walls at or below this ratio should be treated as interacting systems, requiring FEM analysis (e.g., PLAXIS 2D) to accurately capture reduced earth pressures and reinforcement forces, rather than relying on conventional methods, depending on the scale and economy of the project. It is also advised to avoid the use of AASHTO bilinear failure surfaces for flexible-facing walls, as they tend to misrepresent reinforcement behavior.

For detailing in the design, the it is recommended that reinforcement connectivity must be considered, as it reduces displacements and increase the pressure on the facing system, which maintaining the peak tension on the reinforcement.

Future research should expand the study by examining different W/H ratios, wall heights, soil and reinforcement properties, and vehicle load positions to refine the interaction criteria. Key expansions include dynamic loading analysis, broader evaluation of reinforcement connectivity across different spacing ranges, and experimental validation through physical or full-scale BBMSE wall testing. Further work is also recommended on seismic response and long-term creep behavior, to improve the reliability and applicability of BBMSE wall design under real-world conditions.

REFERENCES

AASTHO, & Caltrans. (2017). AASTHO LRFD Bridge Design Specifications. *California Transportation Department*, (2000).

Akbaş, B. (2015). *Probabilistic Slope Stability Analysis Using Limit Equilibrium, Finite Element and Random Finite Element Methods: A Thesis Submitted to the Graduate School of Natural and Applied Sciences of Middle East Technical University*.

Andrawes, K. Z., McGown, A., & Kabir, M. H. (1984a). Uniaxial strength testing of woven and nonwoven geotextiles. *Geotextiles and Geomembranes*, *1*(1). https://doi.org/10.1016/0266-1144(84)90004-9

Andrawes, K. Z., McGown, A., & Kabir, M. H. (1984b). *Uniaxial strength testing of woven and nonwoven geotextiles*.

Baral, P., Bergado, D. T., & Duangkhae, S. (2016). The use of polymeric and metallic geogrid on a full-scale MSE wall/embankment on hard foundation: a comparison of field data with simulation. *International Journal of Geo-Engineering*, *7*(1). https://doi.org/10.1186/s40703-016-0035-6

Bathurst, R. J., Walters, D., Vlachopoulos, N., Burgess, P., & Allen, T. M. (2000). Full scale testing of geosynthetic reinforced walls. *Proceedings of Sessions of Geo-Denver 2000 - Advances in Transportation and Geoenvironmental Systems Using Geosynthetics, GSP 103*, *291*. https://doi.org/10.1061/40515(291)14

Benmebarek, S., Attallaoui, S., & Benmebarek, N. (2016). Interaction analysis of back-to-back mechanically stabilized earth walls. *Journal of Rock Mechanics and Geotechnical Engineering*, *8*(5), 697–702. https://doi.org/10.1016/j.jrmge.2016.05.005

Benmebarek, S., & Djabri, M. (2017). FEM to investigate the effect of overlapping-reinforcement on the performance of back-to-back embankment bridge approaches under self-weight. *Transportation Geotechnics*, *11*, 17–26. https://doi.org/10.1016/j.trgeo.2017.03.002

Benmebarek, S., & Djabri, M. (2018). FE Analysis of Back-to-Back Mechanically Stabilized Earth Walls Under Cyclic Harmonic Loading. *Indian Geotechnical Journal*, *48*(3), 498–509. https://doi.org/10.1007/s40098-017-0269-z

Berg, R. R., Christopher, B. R., & Samtani, N. C. (2009). *Design and Construction of Mechanically Stabilized Earth Walls and Reinforced Soil Slopes-Volume II*.

Binquet, J., & Lee, K. L. (1975). Bearing Capacity Tests on Reinforced Earth Slabs. *ASCE J Geotech Eng Div*, *101*(12). https://doi.org/10.1061/ajgeb6.0000219

Bouacha, N. (2018). Comparison of Geotextile-Reinforced and Geogrid-Reinforced Flexible Pavements by Numerical Analyses. *Sustainable Civil Infrastructures*, 55–69. https://doi.org/10.1007/978-3-319-63570-5_6

Brinkgreve, R. B. J., Waterman, D., Chesaru, A., Bonnier, P. G., & Galavi, V. (2012). *PLAXIS 2D 2012*. www.plaxis.nl

Brouthen, A., Houhou, M. N., & Damians, I. P. (2022). Numerical Study of the Influence of the Interaction Distance, the Polymeric Strips Pre-Tensioning, and the Soil–Polymeric Interaction on the Performance of Back-to-Back Reinforced Soil Walls. *Infrastructures*, *7*(2). https://doi.org/10.3390/infrastructures7020022

Cai, Z., & Bathurst, R. J. (1995). Seismic Response Analysis of Geosynthetic Reinforced Soil Segmental Retaining Walls by Finite Element Method. In *Computers and Geotechnics* (Vol. 17).

Cardoso, A. S., Borges, J. L., Costa, P. A., Gomes, A. T., Marques, J. C., & Vieira, C. S. (Eds.). (2018). *Numerical Methods in Geotechnical Engineering IX*. CRC Press. https://doi.org/10.1201/9781351003629

Chauhan, V. B., Srivastava, A., Jaiswal, S., & Keawsawasvong, S. (2023). Behavior of Back-to-Back MSE Walls: Interaction Analysis Using Finite Element Modeling. *Transportation Infrastructure Geotechnology*, *10*(5), 888–912. https://doi.org/10.1007/s40515-022-00248-0

Christopher, B. R., Gill, S. A., Giroud, J.-P., Juran, Il., Mitchell, J. K., Schlossser, F., & Dunnicliff, J. (1990). *Reinforced Soil Structures Volume I. Design and Construction Guidelines Federal Highway Administration*.

Clough GW, & Duncan JM. (1971). Finite element analyses of retaining wall behavior. *ASCE J Soil Mech Found Div*, *97*(SM12). https://doi.org/10.1061/jsfeaq.0001713

Collop, A. C., Cebon, D., & Hardy, M. S. A. (1995). Viscoelastic approach to rutting in flexible pavements. *Journal of Transportation Engineering*, *121*(1). https://doi.org/10.1061/(ASCE)0733-947X(1995)121:1(82)

Cristelo, N., Félix, C., Lopes, M. L., & Dias, M. (2016). Monitoring and numerical modelling of an instrumented mechanically stabilized earth wall. *Geosynthetics International*, *23*(1), 48–61. https://doi.org/10.1680/jgein.15.00032

Djabri, M., & Benmebarek, S. (2016). FEM Analysis of Back-to-Back Geosynthetic-Reinforced Soil Retaining Walls. *International Journal of Geosynthetics and Ground Engineering*, *2*(3). https://doi.org/10.1007/s40891-016-0067-1

Dov Leshchinsky, B., Member, A., & Boedeker, R. H. (n.d.). *Geosynthetic Reinforced Soil Structures*.

Elias, V., Christopher, B., & Berg, R. (2001). Mechanically Stabilized Earth Walls and Reinforced Soil Slopes Design & Construction Guidelines, Publication No. FHWA-NHI-00-043. *Federal High Way Administration*.

El-Sherbiny, R., Ibrahim, E., & Salem, A. (2013). *Stability of Back-to-Back Mechanically Stabilized Earth Walls*. https://doi.org/10.1061/9780784412787.058

FHWA. (2009a). *Design and Construction of Mechanically Stabilized Earth Walls and Reinforced Soil Slopes-Volume I*.

FHWA. (2009b). *Design and Construction of Mechanically Stabilized Earth Walls and Reinforced Soil Slopes-Volume I*.

Gouw, T.-L. (2018). Common Mistakes in Plaxis-S11-07. *The 11th International Conference on Geosynthetics*.

Groot, M. B. de., Hoedt, G. den., & TerMaat, R. J. . (1996). *Geosynthetics: applications, design and construction*. A.A. Balkema.

Guler, E., Cicek, E., Demirkan, M. M., & Hamderi, M. (2012). Numerical analysis of reinforced soil walls with granular and cohesive backfills under cyclic loads. *Bulletin of Earthquake Engineering*, *10*(3), 793–811. https://doi.org/10.1007/s10518-011-9322-y

Gurung, M., & Acharya, I. P. (n.d.). *Parametric Study of Mechanically Stabilized Earth Wall*.

Ha, N. M., Thanh, P. T., Van, N., & Popov, H. V. (2021). Selection of parameters for MSE retaining walls. *IOP Conference Series: Materials Science and Engineering*, *1030*(1). https://doi.org/10.1088/1757-899X/1030/1/012075

Han, J., & Leshchinsky, D. (2010). Analysis of back-to-back mechanically stabilized earth walls. *Geotextiles and Geomembranes*, *28*(3), 262–267. https://doi.org/10.1016/j.geotexmem.2009.09.012

Hardianto, F. S., & Truong, K. M. (2010). *Seismic Deformation of Back-To-Back Mechanically Stabilized Earth (MSE) Walls*.

Hassan, M. A., Hammad, M. S., & Fayed, A. L. (n.d.). *Behaviour of mechanically stabilized earth wall (MSE) under different cases of loading*.

Hatami, K., & Bathurst, R. J. (2005). Development and verification of a numerical model for the analysis of geosynthetic-reinforced soil segmental walls under working stress conditions. *Canadian Geotechnical Journal*, *42*(4), 1066–1085. https://doi.org/10.1139/t05-040

Hatami, K., & Bathurst, R. J. (2006). Numerical Model for Reinforced Soil Segmental Walls under Surcharge Loading. *Journal of Geotechnical and Geoenvironmental Engineering*, *132*(6). https://doi.org/10.1061/(asce)1090-0241(2006)132:6(673)

Helwany, S. M. B., Reardon, G., & Wu, J. T. H. (1999). Effects of backfill on the performance of GRS retaining walls. *Geotextiles and Geomembranes*, *17*(1). https://doi.org/10.1016/S0266-1144(98)00021-1

Helwany, S. M. B., Wu, J. T. H., & Froessl, B. (2003). GRS bridge abutments - An effective means to alleviate bridge approach settlement. *Geotextiles and Geomembranes*, *21*(3), 177–196. https://doi.org/10.1016/S0266-1144(03)00004-9

Huang, B., Bathurst, R. J., Hatami, K., & Asce, M. (2009). Numerical Study of Reinforced Soil Segmental Walls Using Three Different Constitutive Soil Models. *J. Geotech. Geoenviron. Eng.* https://doi.org/10.1061/ASCEGT.1943-5606.0000092

Hunaidi, O., Guan, W., & Nicks, J. (2000). Building vibrations and dynamic pavement loads induced by transit buses. *Soil Dynamics and Earthquake Engineering*, *19*(6). https://doi.org/10.1016/S0267-7261(00)00019-1

International • ; Abu-Hejleh, G., Zornberg, N. G., Wang, J. G., & Watcharamonthein, T. (2002). Monitored Displacements of Unique Geosynthetic-Reinforced Soil Bridge Abutments. In *Geosynthetics International* (Vol. 9, Number 1).

International S ; Bathurst, G., & Cai, R. J. (1995). Pseudo-Static Seismic Analysis of Geosynthetic-Reinforced Segmental Retaining Walls. In *Geosynthetics International* (Vol. 2, Number 5).

Jewell, R. A., & Greenwood, J. H. (1988). Long term strength and safety in steep soil slopes reinforced by polymer materials. *Geotextiles and Geomembranes*, *7*(1–2). https://doi.org/10.1016/0266-1144(88)90020-9

Jewell, R. A., Milligan, G. W. E., Sarsby, R. W., & Dubois, D. (1984). *Interaction Between Soil and Geogrids.*

Jiang, Y. (2016). *Evaluating Performance of Hybrid Geosynthetic-Reinforced Retaining Walls*.

Juneja, A., Joseph, A., & Murty, D. S. (2025). *GeoVadis*. CRC Press. https://doi.org/10.1201/9781003645931

Kakrasul, J. I., Han, J., & Rahmaninezhad, S. M. (2020). Load-Deformation Behavior of Geosynthetic-Reinforced Retaining Walls with Limited Fill Space Under Static Footing Loading. *Transportation Infrastructure Geotechnology*, *7*(3). https://doi.org/10.1007/s40515-020-00132-9

Khan, M., Umar, M., Alam, M., Ali, U., Vatin, N. I., & Almujibah, H. (2024). Evaluation of design parameters for geosynthetic reinforced-soil integrated bridge system based on finite element analysis. *Frontiers in Materials*, *11*. https://doi.org/10.3389/fmats.2024.1454201

Khoury, C. N., Miller, G. A., & Hatami, K. (2011). Unsaturated soil-geotextile interface behavior. *Geotextiles and Geomembranes*, *29*(1). https://doi.org/10.1016/j.geotexmem.2010.06.009

Kibria, G., Asce, S. M., Hossain, M. S., Asce, M., & Khan, M. S. (2014). *Influence of Soil Reinforcement on Horizontal Displacement of MSE Wall*. https://doi.org/10.1061/(ASCE)GM.1943

Koerner, R. M. (2005). *Designing with geosynthetics*. Pearson Prentice Hall.

Koerner, R. M., & Soong, T.-Y. (2001). Geosynthetic reinforced segmental retaining walls. In *Geotextiles and Geomembranes* (Vol. 19).

Kongkitkul, W., Tatsuoka, F., Hirakawa, D., Sugimoto, T., Kawahata, S., & Ito, M. (2010). Time histories of tensile force in geogrid arranged in two full-scale high walls. *Geosynthetics International*, *17*(1). https://doi.org/10.1680/gein.2010.17.1.12

Lajevardi, S. H., Malekmohammadi, K., & Dias, D. (2021). Numerical Study of the Behavior of Back-to-Back Mechanically Stabilized Earth Walls. *Earth Walls. Geotechnics*, *2021*, 18–37. https://doi.org/10.3390/geotechnics

Langcuyan, C. P., Gao, Y.-C., & Won, M.-S. (n.d.). *Effects of surface vibrations on the behavior of panel-type MSE walls*.

Langcuyan, C. P., Sadiq, S., Park, T. W., & Won, M. S. (2023). Dynamic analysis of MSE wall subjected to surface vibration loading. *Open Geosciences*, *15*(1). https://doi.org/10.1515/geo-2022-0592

Leshchinsky, D., & Han, J. (2004). Geosynthetic Reinforced Multitiered Walls. *Journal of Geotechnical and Geoenvironmental Engineering*, *130*(12), 1225–1235. https://doi.org/10.1061/(asce)1090-0241(2004)130:12(1225)

Li, F., Guo, W., Pu, H., & Zheng, Y. (2024). Influence of geometric configuration on the deformation behavior of back-to-back MSE walls under dynamic loading. *Japanese Geotechnical Society Special Publication*, *10*(25), 914–917. https://doi.org/10.3208/jgssp.v10.os-14-01

Li, F., Guo, W., & Zheng, Y. (2023). Influence of geometric configuration on the interaction of back-to-back MSE walls under static loading. In *Geosynthetics: Leading the Way to a Resilient Planet* (pp. 948–953). CRC Press. https://doi.org/10.1201/9781003386889-114

Ling, H. I., Asce, M., Liu, H., Kaliakin, V. N., & Leshchinsky, D. (n.d.). *Analyzing Dynamic Behavior of Geosynthetic-Reinforced Soil Retaining Walls*. https://doi.org/10.1061/ASCE0733-93992004130:8911

Ling, H. I., Leshchinsky, Ã. D., & Perry, E. B. (1997). *Seismic design and performance of geosynthetic-reinforced soil structures*.

Ling, H. I., Leshchinsky, D., & Chou, N. N. S. (n.d.). *Post-earthquake investigation on several geosynthetic-reinforced soil retaining walls and slopes during the Ji-Ji earthquake of Taiwan*. Retrieved www.elsevier.com/locate/soildyn

Lombaert, G., Degrande, G., Kogut, J., & François, S. (2006). The experimental validation of a numerical model for the prediction of railway induced vibrations. *Journal of Sound and Vibration*, *297*(3–5). https://doi.org/10.1016/j.jsv.2006.03.048

Lysmer, J., & Kuhlemeyer, R. L. (1969). Finite Dynamic Model for Infinite Media. *Journal of the Engineering Mechanics Division*, *95*(4). https://doi.org/10.1061/jmcea3.0001144

Madhavi Latha, G., & Murali Krishna, A. (2008). Seismic response of reinforced soil retaining wall models: Influence of backfill relative density. *Geotextiles and Geomembranes*, *26*(4), 335–349. https://doi.org/10.1016/j.geotexmem.2007.11.001

Mahmood, T. (2009a). *Failure Analysis of a Mechanically Stabilized Earth (MSE) Wall Using Finite Element Program Plaxis*.

Mahmood, T. (2009b). *Failure Analysis of a Mechanically Stabilized Earth (MSE) Wall Using Finite Element Program Plaxis*.

McGown, A. (1982). *Load/extension testing of geotextiles confined in-soil*.

Mitchell, J. K., & Villet, W. C. B. (1987). Reinforcement of Earth Slopes and Embankments. *National Cooperative Highway Research Program Report*.

Miura, N., Ochiai, H., & Yamanouchi, T. (2026). *Theory and Practice of Earth Reinforcement*. CRC Press. https://doi.org/10.1201/9781003763314

Mukunoki, T., Otani, J., & Miyata, Y. (2023). *New Horizons in Earth Reinforcement*. CRC Press. https://doi.org/10.1201/9781003416753

Naylor, D. J. (1982). Finite Elements and Slope Stability. In J. B. Martins (Ed.), *Numerical Methods in Geomechanics* (pp. 229–244). Springer Netherlands.

Ochiai, H., Yasufuku, N., & Omine, K. (2026). *Earth Reinforcement, volume 1*. CRC Press. https://doi.org/10.1201/9781003761624

Ochiai, Hidetoshi., Hayashi, Shigenori., & Ōtani, Jun. (1993). *Earth reinforcement practice: proceedings of the International Symposium on Earth Reinforcement Practice, Fukuoka, Kyushu, Japan, 11-13 November 1992*. A.A. Balkema.

Paulsen, S. B., & Kramer, S. L. (2004). A predictive model for seismic displacement of reinforced slopes. In *Geosynthetics International* (Vol. 11, Number 6).

Prashad, D., Shubham, K., Metya, S., & Singh, R. P. (2025). Major Developments and Improvements in Mechanically Stabilized Earth (MSE) Walls: Analysis and Design over the last three decades Author names and affiliations. *Civil*

Engineering Infrastructures Journal. https://doi.org/10.22059/ceij.2025.391083.2258

Rajagopal, G., & Thiyyakkandi, S. (2021). Numerical evaluation of the performance of back-to-back MSE walls with hybrid select-marginal fill zones. *Transportation Geotechnics*, *26*. https://doi.org/10.1016/j.trgeo.2020.100445

Rowe, R. K., & Ho, S. K. (1998). Horizontal deformation in reinforced soil walls. *Canadian Geotechnical Journal*, *35*(2). https://doi.org/10.1139/t97-062

Sandri, D. (1997). A Performance Summary of Reinforced Soil Structures in the Greater Los Angeles Area after the Northridge Earthquake. In *Geotextiles andGeomernbranes* (Vol. 15).

Schlosser, F., & Long, N.-T. (1974). Recent Results of French Research on Reinforced Earth. *Journal of the Construction Division*, *100*(3). https://doi.org/10.1061/jcceaz.0000429

Seed, R., Collin, J., & Mitchell, J. (1986). FEM analyses of compacted reinforced soils. *Proceedings of the Second Symposium on Numerical Models in Geomechanics. Balkema, Rotterdam*, 553–562.

Shukla, S. K., & Yin, J.-H. (2006). *Fundamentals of Geosynthetic Engineering*. Taylor & Francis Group, London, UK.

Sravanam, S. M., Balunaini, U., & Madhav, M. R. (2019). Behavior and Design of Back-to-Back Walls Considering Compaction and Surcharge Loads. *International Journal of Geosynthetics and Ground Engineering*, *5*(4). https://doi.org/10.1007/s40891-019-0180-z

Sravanam, S. M., Balunaini, U., & Madhira, R. M. (2020). Behavior of Connected and Unconnected Back-to-Back Walls for Bridge Approaches. *International Journal of Geomechanics*, *20*(7). https://doi.org/10.1061/(ASCE)GM.1943-5622.0001692

State, W., Holtz, R. D., & Lee, W. F. (2002a). *Internal Stability Analyses of Geosynthetic Reinforced Retaining Walls*.

State, W., Holtz, R. D., & Lee, W. F. (2002b). *Research Report Agreement No.T9903, Task 95 Geosynthetic Reinforcement III INTERNAL STABILITY ANALYSES OF GEOSYNTHETIC REINFORCED RETAINING WALLS*.

Sundaravel, V., & Dodagoudar, G. R. (2024). Finite Element Analysis of Reinforced Earth Retaining Structures: Material Models and Performance Assessment.

Indian Geotechnical Journal, *54*(6), 2076–2095. https://doi.org/10.1007/s40098-023-00839-9

Taylor, T. P., Collin, J. G., Boyle, S., Fishman, K., & Han, J. (2023). *Design and Construction of Mechanically Stabilized Earth (MSE) Walls FHWA GEC 011*. http://www.ntis.gov

Tomar, A., Lohar, J., & Shrivastava, N. (2024). Parametric Study of Mechanically Stabilised Earth Wall using PLAXIS. *IOP Conference Series: Earth and Environmental Science*, *1326*(1). https://doi.org/10.1088/1755-1315/1326/1/012126

Vidal, H. (1966). *The Principle of Reinforced Earth*.

Wartman, J., Asce, M., Rondinel-Oviedo, E. A., & Rodriguez-Marek, A. (n.d.). *Performance and Analyses of Mechanically Stabilized Earth Walls in the Tecomán, Mexico Earthquake*. https://doi.org/10.1061/ASCE0887-3828200620:3287

Won, M. S., & Kim, Y. S. (2007). Internal deformation behavior of geosynthetic-reinforced soil walls. *Geotextiles and Geomembranes*, *25*(1). https://doi.org/10.1016/j.geotexmem.2006.10.001

Won, M. S., & Langcuyan, C. P. (2020). A 3D numerical analysis of the compaction effects on the behavior of panel-type MSE walls. *Open Geosciences*, *12*(1), 1704–1724. https://doi.org/10.1515/geo-2020-0192

Won, M. S., Langcuyan, C. P., Lim, J. H., Nam, S. B., Ham, T. G., & Ha, M. B. (2022). Numerical Analysis of the Deformation Behavior of Geogrid-Reinforced MSE Wall Having FHR and SPT Wall Facing. *Civil Engineering and Architecture*, *10*(5), 2187–2203. https://doi.org/10.13189/cea.2022.100537

Wu, J. T. H. . (2019). *Geosynthetic reinforced soil (GRS) walls*. John Blackwell.

Zevgolis, I., & Bourdeau, P. (2007). *Mechanically Stabilized Earth Wall Abutments for Bridge Support*. https://doi.org/10.5703/1288284313451

Zevgolis, I. E. (2018). A Finite Element Investigation on Displacements of Reinforced Soil Walls Under the Effect of Typical Traffic Loads. *Transportation Infrastructure Geotechnology*, *5*(3), 231–249. https://doi.org/10.1007/s40515-018-0059-9

Zornberg, J. G. (n.d.). *New Concepts in Geosynthetic-Reinforced Soil*.

Zornberg, J. G., & Morsy, A. M. (2024). *Technical Workshop on Reinforcement and Drainage in Soil Structures*.

This page is intentionally left blank.

ANNEX-I: CONNECTIVITY PLOT BBMSE WALL CONFIGURATIONS

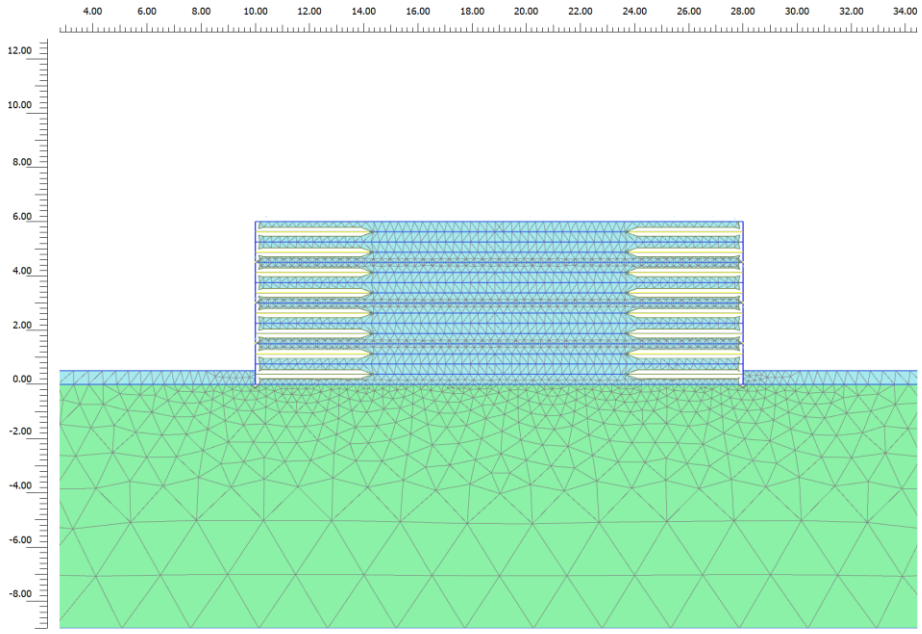

(a) W/H=3.0

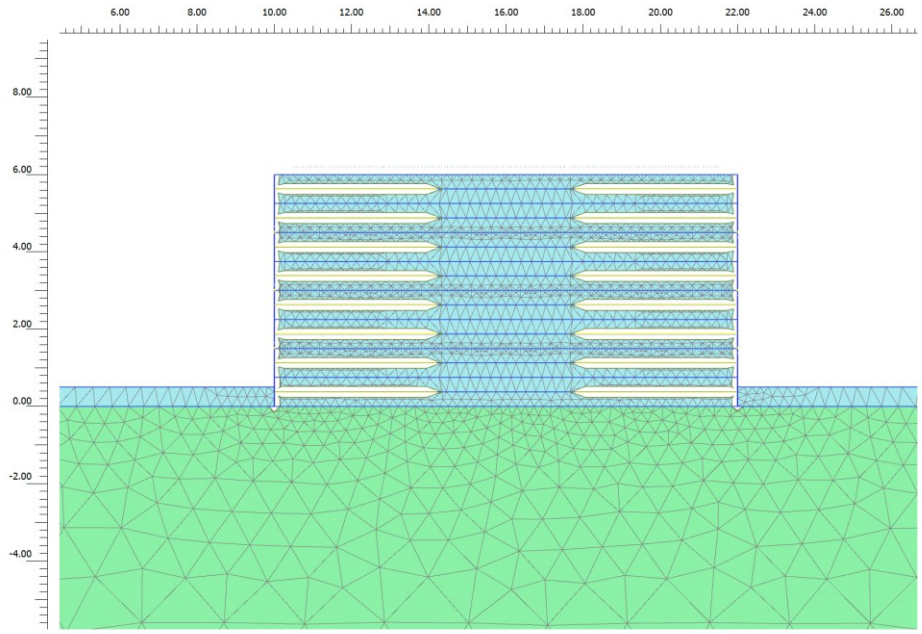

(b) W/H=2.0

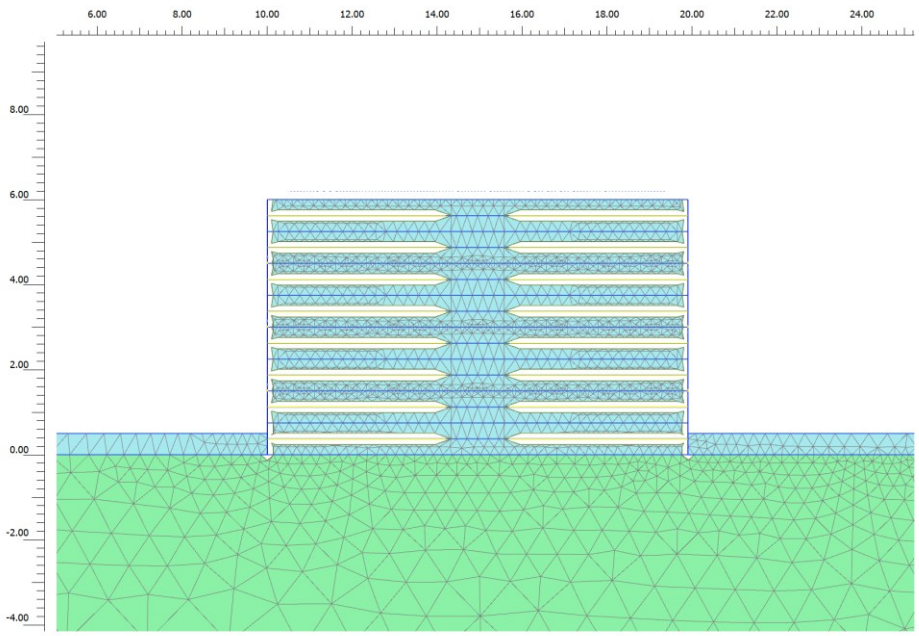
6.00
8.00
10.00
12.00
14.00
16.00
18.00
20.00
22.00
24.00
8.00
6.00
4.00
2.00
0.00
-2.00
-4.00

(c) W/H=1.7

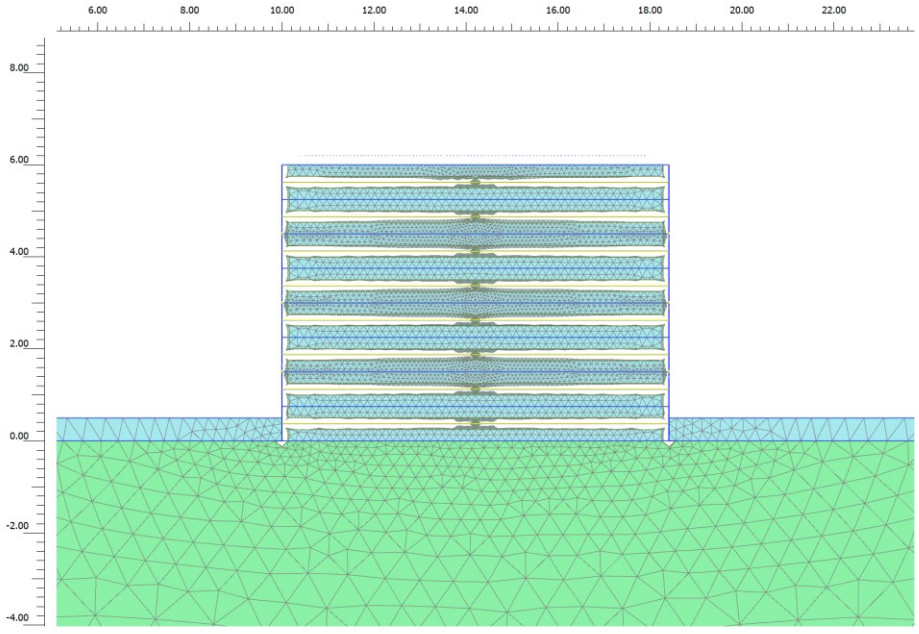
6.00
8.00
10.00
12.00
14.00
16.00
18.00
20.00
22.00
8.00
6.00
4.00
2.00
0.00
-2.00
-4.00

(d) W/H=1.4

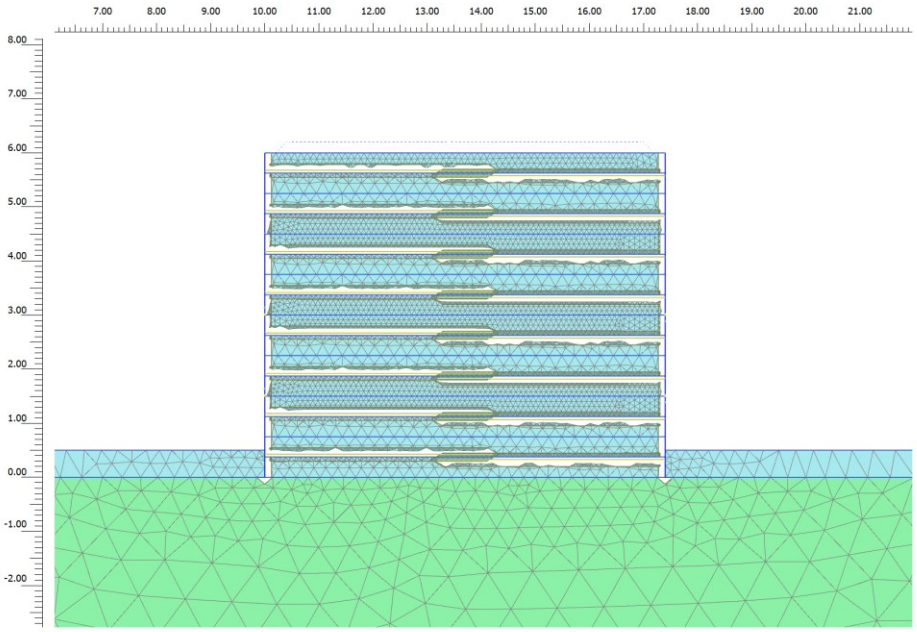

(e) W/H=1.2

Figure: Connectivity Plot of the model in Plaxis 2D

ANNEX-II: LIST OF PUBLICATION

Conference Paper

Giri, K., & Tiwari, R. C. (2026). FEM based performance evaluation of BBMSE walls under static and vehicle surcharge load conditions. *18th IOE Graduate Conference*, Lalitpur, Nepal.